Submillimeter spatial oscillations of Newton's constant:
Theoretical models and laboratory tests

L. Perivolaropoulos[*]

Department of Physics, University of Patras, 26500 Patras, Greece
(Received 25 November 2016; published 27 April 2017)

We investigate the viability of submillimeter-wavelength oscillating deviations from the Newtonian potential at both the theoretical and the experimental/observational level. At the theoretical level, such deviations are generic predictions in a wide range of extensions of general relativity (GR) including $f(R)$ theories, massive Brans-Dicke (BD) scalar-tensor theories, compactified extra dimension models, and nonlocal extensions of GR. However, the range of parameters associated with such oscillating deviations is usually connected with instabilities present at the perturbative level. An important exception emerges in nonlocal gravity theories where oscillating deviations from Newtonian potential occur naturally on submillimeter scales without any instabilities. As an example of a model with unstable Newtonian oscillations, we review an $f(R)$ expansion around general relativity of the form $f(R) = R + \frac{1}{6m^2} R^2$ with $m^2 < 0$, pointing out possible stabilization mechanisms. As an example of a model with stable Newtonian oscillations, we discuss nonlocal gravity theories. If such oscillations are realized in nature on submillimeter scales, a signature is expected in torsion balance experiments testing the validity of Newton's law. We search for such a signature in the torsion balance data of the Washington experiment [D. J. Kapner, T. S. Cook, E. G. Adelberger, J. H. Gundlach, B. R. Heckel, C. D. Hoyle, and H. E. Swanson, Phys. Rev. Lett. **98**, 021101 (2007).] (combined torque residuals of experiments I, II, and III), testing Newton's law at submillimeter scales. We show that an oscillating residual ansatz with spatial wavelength $\lambda \simeq 0.1$ mm provides a better fit to the data compared to the residual Newtonian constant ansatz by $\Delta\chi^2 = -15$. Similar improved fits however, also occur in about 10% of the Monte Carlo realization of Newtonian data on similar or larger scales. Thus, the significance level of this improved fit is at a level of not more than 2σ. The energy scale corresponding to this best-fit wavelength is identical to the dark energy length scale, $\lambda_{de} \equiv \sqrt{4}\hbar c/\rho_{de} \approx 0.1$ mm.

I. INTRODUCTION

The discovery of the accelerating expansion of the Universe [1–3] has opened a new prospect for a possible need for modification of general relativity beyond the level of a cosmological constant. Such a geometric origin of dark energy is simple and well motivated physically [4–8].

The typical physics scale of geometric dark energy required so that it starts dominating the Universe at recent cosmological times is $\lambda_{de} \equiv \sqrt{4}\hbar c/\rho_{de} \approx 0.085$ mm (assuming $\Omega_{0m} = 0.3$ and $H_0 = 70$ km sec^{-1} Mpc^{-1}). Therefore, if the origin of the accelerating expansion is geometrical, it is natural to expect the presence of signatures of modified gravity on scales of about 0.1 mm.

A wide range of experiments has focused on this range of scales [9–12], and constraints have been imposed on particular parametrizations of extensions of Newton's gravitational potential. Such parametrizations are motivated by viable extensions of general relativity and include

Yukawa interactions leading to an effective gravitational potential

$$V_{\text{eff}} = -G\frac{M}{r}(1 + \alpha e^{-mr}) \tag{1.1}$$

and a power-law ansatz of the form [13]

$$V_{\text{eff}} = -G\frac{M}{r}\left(1 + \beta^k \left(\frac{1}{mr}\right)^{k-1}\right) \tag{1.2}$$

arising, for example, in the context of some brane world models [14–17].

The Yukawa interaction parametrization (1.1) is motivated by the weak gravitational field limit solution of a point mass in a wide range of extensions of GR, including $f(R)$ theories [18–20], massive Brans-Dicke (BD) [21–23] and scalar-tensor theories, compactified extra dimension models [24–29], etc. In each of these models, the mass scale m has a different physical origin. For example, in massive BD theories, m is the mass scale of the BD scalar, and $\alpha = \frac{1}{3+2\omega}$; while in $f(R)$ theories, it is the lowest-order-term series expansion of $f(R)$ around GR of the form

[*]leandros@uoi.gr
On leave from the Department of Physics, University of Ioannina, 45110 Ioannina, Greece.

$$f(R) = R + \frac{1}{6m^2}R^2 + \cdots. \qquad (1.3)$$

In $f(R)$ theories, we have $\alpha = \frac{1}{3}$ [30]. In radion compactified extra dimension models, m is the inverse radius of the extra dimension ($m = b^{-1}$), while $\alpha = \frac{D}{D+2}$ [27], where D is the number of toroidally compactified dimensions even though different values may be obtained for different compactifications [29].

In all these theories, the weak-field-limit solution remains mathematically valid and consistent for $m^2 < 0$ [18,30]. For this mass range, the correction of the effective gravitational potential becomes oscillating and takes the form

$$V_{\text{eff}} = -G\frac{M}{r}(1 + \alpha\cos(mr + \theta)), \qquad (1.4)$$

where θ is an arbitrary parameter. Such a potential clearly has no Newtonian limit and could be ruled out immediately on this basis [20,31]. However, since the extra force component averages out to zero, for submillimeter wavelength oscillations and $\alpha = O(1)$, such an oscillating correction could remain undetectable by current experiments and astrophysical observations due to finite accuracy in length and force measurements.

This class of theories however, has an additional problem: the vacuum in most such theories suffers from serious instabilities [32,33] (see also Ref. [34]) in this range of values of m^2. Due to these problems, the oscillating correction has not been considered in any detail, and there are currently no experimental constraints on the corresponding parametrization parameters.

A peculiar feature of these perturbative results [32,33,35–40] is that they indicate the presence of an infinite discontinuity in the stability properties of these theories as $m^{-2} \to 0^-$. In this limit, $f(R)$ theories are extremely unstable (with a lifetime of the vacuum that approaches zero as $m^{-2} \to 0$). At exactly $m^{-2} = 0$, however, the theory becomes stable and identical to GR. The existence of this unphysical infinite discontinuity may indicate that nonperturbative effects and nontrivial backgrounds may play a significant role in the stability analysis. Such effects are briefly discussed in the present analysis.

A more promising theoretical model where stable spatial oscillations naturally occur for the gravitational potential are nonlocal theories of gravity [41–43] motivated from string theory and described by actions that are made generally covariant and ghost-free at the perturbative level by including infinite derivatives [44–46]. For example, such an action, viable also at the cosmological level, is of the form [47]

$$S = \frac{1}{16\pi G}\int d^4x\sqrt{-g}\left[R + \frac{1}{6m^2}R\left(1 - \frac{\Lambda^4}{\Box^2}\right)R\right], \qquad (1.5)$$

where m is the scale of nonlocality and $\Box$ is the d'Alembert operator.

In this class of theories, the generalized Newtonian potential remains finite at $r = 0$ and may develop spatial oscillations [41,42,48] around the scale of nonlocality (see Sec. II C) which decay on larger scales. Despite its increased complexity, this class of theories has four important advantages:

(1) They can be free from singularities while having a proper Newtonian limit [43].
(2) They are free from instabilities in the absence of tensorial nonlocal terms [49].
(3) They can emerge from effects at the quantum level. In particular, light-particle loops at the quantum level can generate nonlocal terms in the quantum effective action, which can make it renormalizable [50].
(4) They are consistent with the cosmological observations without need for a cosmological constant [47,51–53].

Thus, in view of the generic nature of oscillating parametrizations and the fact that there may be stabilization mechanisms like backreaction from higher-order nonlinear or nonlocal terms, it is of interest to consider in some detail the theoretical models and the observational consequences of such an oscillating correction of Newton's law potential. This is the goal of the present analysis.

A wide range of experiments (see Fig. 1 and Ref. [10] for a good review) have been performed during recent years, imposing constraints on deviations from Newton's law using the Yukawa and the power-law parametrizations. These include torsion balance experiments [54–69] measuring gravitational torques from source masses on test masses attached to torsion balance bars, Casimir force experiments [70,71] looking for anomalies in the electric
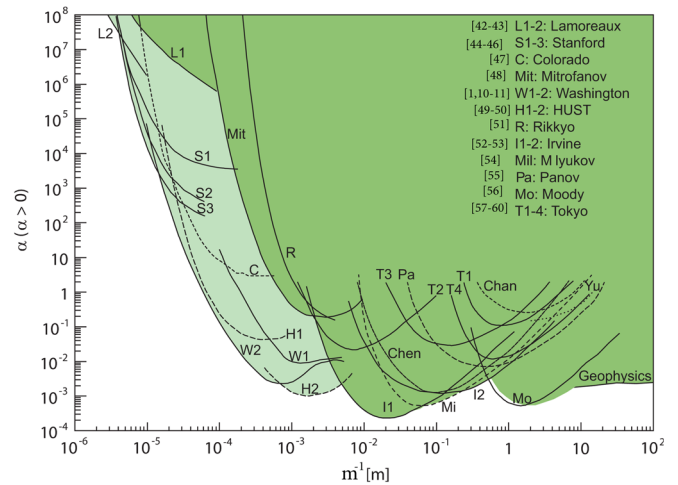

FIG. 1. A review of current constraints [9,11,12,54–67,70,71, 73–75] based on the Yukawa parametrization (1.1) for deviation from Newton's law (from Ref. [10]).

forces between two metal surfaces and atomic or nuclear experiments [72], and looking for anomalies in the dynamical evolution of particle systems in the context of known standard-model interactions. The constraints of such experiments on Yukawa deviations from a Newtonian potential are reviewed in Fig. 1.

The most constraining experiments testing the Yukawa parametrization (1.1) for deviations from Newton's law for $\alpha = O(1)$ have been performed using a torsion balance instrument by the Washington group [9] in 2006. For $\alpha = 1$, the 2σ constraint on m was obtained as $m \gtrsim 18$ mm^{-1}. An interesting open question is the following: What are corresponding constraints in the context of an oscillating parametrization for deviations from Newton's law? The answer to this question is one of the main goals of the present analysis.

The structure of this paper is the following: In the next section, we discuss the emergence of an oscillating deviation from Newton's constant in a particular class of theoretical modified gravity models: $f(R)$ theories [76] with $f(R) = R + \frac{1}{6m^2}R^2$. We derive the parameter range of m^2 for which an oscillating deviation from the Newtonian potential emerges using both the $f(R)$ formalism [77] and the equivalent massive BD formalism [78]. We also discuss the stability of this solution and confirm that it is unstable, in accordance with the Dolgov-Kawasaki-Faraoni instability [32,38]. The gravitational potential that emerges in nonlocal gravity theories is also discussed and shown to have oscillating deviations from the Newtonian potential. Even though these deviations are in general complicated functional expressions [41], we show that within appropriate limits, they are very well fit by simple trigonometric functions. In Sec. III, we discuss the consistency of these submillimeter oscillations of the generalized Newtonian potential with macroscopic large-scale observations given the finite accuracy in the measurement of forces and lengths. We also use an oscillating parametrization to fit the torsion balance data of the Washington group experiment. Finally, in Sec. IV, we conclude, summarize, and discuss future extensions of the present analysis.[1]

II. SPATIAL OSCILLATIONS OF NEWTON'S CONSTANT IN MODIFIED GRAVITY THEORIES

A. $f(R)$ theories I: The equivalent BD formalism and the Newtonian limit

The Einstein-Hilbert action is generalized in the context of $f(R)$ theories as

---

[1]In what follows, we use the metric signature $(-+++)$. This is important, in view of the fact that the sign of the Ricci scalar changes if a different metric signature is used, and thus the sign of m^2 in Eq. (1.3) leading to stability or instability would also change.

$$S_R = \frac{1}{16\pi G} \int d^4x \sqrt{-g} f(R) + S_{\text{matter}}, \qquad (2.1)$$

where R is the Ricci scalar. This action may be shown to be dynamically equivalent to the scalar-tensor action of a massive BD scalar field with $\omega = 0$ [78–80]:

$$S_{BD} = \frac{1}{16\pi G} \int d^4x \sqrt{-g} [f(\phi) + f_\phi(\phi)(R - \phi)] + S_{\text{matter}}. \tag{2.2}$$

Variation of the action (2.2) with respect to the field ϕ leads to the condition $\phi = R$ (assuming $f_{\phi\phi} \neq 0$), which reduces the action (2.2) to the $f(R)$ action (2.1) [78]. Assuming an $f(R)$ theory of the form

$$f(R) = R + \frac{1}{6m^2}R^2, \qquad (2.3)$$

the scalar field action (2.2) is easily shown to take the form

$$S_{BD} = \frac{1}{16\pi G} \int d^4x \sqrt{-g} \left[\left(1 + \frac{1}{3m^2}\phi \right) R - \frac{1}{6m^2}\phi^2 \right] + S_{\text{matter}}. \tag{2.4}$$

We now define the field $\Phi \equiv 1 + \frac{1}{3m^2}\phi$, and the action (2.4) takes the form

$$S_{BD} = \frac{1}{16\pi G} \int d^4x \sqrt{-g} \left[\Phi R - \frac{3}{2}m^2(\Phi - 1)^2 \right] + S_{\text{matter}}. \tag{2.5}$$

The action (2.5) is identical with the action of a massive BD scalar field with $\omega = 0$. Due to the nonzero mass of the BD scalar PPN parameter, γ is not of the form $\gamma = \frac{1+\omega}{2+\omega} = \frac{1}{2}$ as in the massless case. The Newtonian limit of this theory has been investigated in detail in Ref. [21], but we review that analysis here for completeness, setting $\omega = 0$.

The dynamical field equations obtained by varying the action (2.5) are of the form

$$\Phi \left(R_{\mu\nu} - \frac{1}{2}g_{\mu\nu}R \right) = 8\pi G T_{\mu\nu} + \nabla_\mu \partial_\nu \Phi - g_{\mu\nu}\Box\Phi$$
$$- g_{\mu\nu}\frac{3}{4}m^2(\Phi - 1)^2 \qquad (2.6)$$

$$\Box\Phi = \frac{8\pi G}{3}T + m^2((\Phi - 1)^2 + (\Phi - 1)\Phi). \qquad (2.7)$$

We now consider the weak gravitational field of a point mass with

$$T_{\mu\nu} = \text{diag}(M\delta(\vec{r}), 0, 0, 0), \qquad (2.8)$$

and thus we expand around a constant-uniform background field $\Phi_0 = 1$ and a Minkowski metric $\eta_{\mu\nu} = \text{diag}(-1, 1, 1, 1)$:

$$\Phi = 1 + \varphi, \tag{2.9}$$

$$g_{\mu\nu} = \eta_{\mu\nu} + h_{\mu\nu}. \tag{2.10}$$

The resulting equations for φ and $h_{\mu\nu}$ obtained from (2.6), (2.7), (2.9), and (2.10) in the gauge $h^{\mu}_{\nu,\mu} - \frac{1}{2} h^{\mu}_{\mu,\nu} = \varphi_{,\nu}$ are of the form

$$(\Box - m^2)\varphi = -\frac{8\pi G}{3} M\delta(\vec{r}), \tag{2.11}$$

$$-\frac{1}{2}\left[\Box\left(h_{\mu\nu} - \eta_{\mu\nu}\frac{h}{2}\right)\right] = 8\pi G T_{\mu\nu} + \partial_\mu\partial_\nu\varphi - \eta_{\mu\nu}\Box\varphi, \tag{2.12}$$

where $h = h^{\mu}_{\mu}$. For static configurations, the equations (2.11) and (2.12) become

$$\nabla^2\varphi - m^2\varphi = -\frac{8\pi G}{3} M\delta(\vec{r}), \tag{2.13}$$

$$\nabla^2 h_{00} - \nabla^2\varphi = -8\pi GM\delta(\vec{r}), \tag{2.14}$$

$$\nabla^2 h_{ij} - \delta_{ij}\nabla^2\varphi = -8\pi GM\delta(\vec{r})\delta_{ij}. \tag{2.15}$$

These equations have the following solution:

$$\varphi = \frac{2GM}{3r} e^{-mr}, \tag{2.16}$$

$$h_{00} = \frac{2GM}{r}\left(1 + \frac{1}{3}e^{-mr}\right), \tag{2.17}$$

$$h_{ij} = \frac{2GM}{r}\delta_{ij}\left(1 - \frac{1}{3}e^{-mr}\right). \tag{2.18}$$

The metric may now be expanded in terms of the γ post-Newtonian parameter as

$$g_{00} = -(1 + 2V_{\text{eff}}), \tag{2.19}$$

$$g_{ij} = (1 - 2\gamma V_{\text{eff}})\delta_{ij}, \tag{2.20}$$

where V_{eff} is the Newtonian potential. Thus, we obtain

$$\gamma(m, r) = \frac{h_{ij}|_{i=j}}{h_{00}} = \frac{3 - e^{-mr}}{3 + e^{-mr}}. \tag{2.21}$$

In the special case of $m = 0$, we obtain the result of Refs. [77,81–83], $\gamma = \frac{1}{2}$ (extreme deviation from GR); while for $m \to \infty$, we recover the GR limit $\gamma \to 1$. It is

therefore clear that these theories are viable and have a well-defined Newtonian limit in contrast to the conclusion of some previous studies (e.g. Ref. [77]).

The generalized Newtonian potential takes the form

$$V_{\text{eff}} = -\frac{h_{00}}{2} = -\frac{GM}{r}\left(1 + \frac{1}{3}e^{-mr}\right), \tag{2.22}$$

while the corresponding force is

$$\overrightarrow{F}_{\text{eff}} = -\hat{r}\frac{GM}{r^2}\left(1 + \frac{e^{-mr}}{3} + \frac{mr}{3}e^{-mr}\right). \tag{2.23}$$

The stability of the solution in (2.16)–(2.18) may be studied by considering perturbations of the form $\varphi = \varphi_0(r) + \delta\varphi(r, t)$, where φ_0 is the unperturbed static solution (2.16). The perturbation satisfies the equation

$$-\ddot{\delta\varphi} + \nabla^2\delta\varphi - m^2\delta\varphi = 0. \tag{2.24}$$

For $m^2 > 0$, this is the Klein-Gordon equation, which has only wavelike solutions, and therefore φ_0 is stable. The presence of higher-order terms in the Lagrangian (2.5), however, could change the stability properties of this solution, since it is well known that the nonlinear Klein-Gordon equation can have instabilities around nontrivial solutions (e.g. Ref. [84]). The vacuum solution, however, ($\varphi = 0$) is always stable for $m^2 > 0$.

For $m^2 < 0$, the weak-field solution of Eq. (2.13) becomes oscillatory and takes the form

$$\varphi = \frac{2GM}{3r}\cos(|m|r + \theta), \tag{2.25}$$

where θ is an arbitrary phase. The Newtonian potential in this case takes the form

$$V_{\text{eff}} = -\frac{h_{00}}{2} = -\frac{GM}{r}\left(1 + \frac{1}{3}\cos(|m|r + \theta)\right). \tag{2.26}$$

This solution is perturbatively unstable in the absence of higher-order terms in the action or in the absence of a nontrivial background energy-momentum tensor. In addition, the trivial vacuum solution ($\varphi_0 = 0$) is clearly always unstable for this range of m^2.

B. $f(R)$ theories II: The Newtonian limit in the $f(R)$ formalism

We now rederive the form of the weak-field metric and the effective Newtonian potential using the $f(R)$ formalism directly [18,19,30,77,78,81,85], since there has been some controversy in the literature concerning the equivalence of the two formalisms [80].

Variation of the $f(R)$ action (2.1) with respect to the metric leads to the generalized Einstein equations

$$f'(R)R_{\mu\nu} - \frac{1}{2}g_{\mu\nu}f(R) = 8\pi G T_{\mu\nu} + \nabla_\mu\nabla_\nu f'(R)$$
$$- g_{\mu\nu}\Box f'(R). \qquad (2.27)$$

Using the ansatz (2.3) and the weak-field metric expansion (2.10) while keeping only linear terms in $h_{\mu\nu}$, the dynamical equations take the form

$$R_{\mu\nu} - \frac{1}{2}R\eta_{\mu\nu} = 8\pi G T_{\mu\nu} + (\partial_\mu\partial_\nu - \eta_{\mu\nu}\nabla^2)\frac{1}{3m^2}R. \quad (2.28)$$

Taking the trace of (2.28) and using Eq. (2.8), we find

$$\frac{1}{m^2}\nabla^2 R - R = -8\pi GM\delta(\vec{r}). \qquad (2.29)$$

For $m^2 > 0$, the physically interesting solution of this equation is

$$\bar{R} = \frac{2GM}{r}m^2 e^{-mr}, \qquad (2.30)$$

while for $m^2 < 0$, we obtain the oscillating form

$$\bar{R} = \frac{2GM}{r}m^2 \cos(|m|r + \theta). \qquad (2.31)$$

Using Eq. (2.30) in Eq. (2.28), we now find the equation for the 00-component as

$$R_{00} = \frac{16}{3}\pi G\rho - \frac{1}{6}R. \qquad (2.32)$$

At the linear level in $h_{\mu\nu}$, the Ricci tensor is of the form

$$R_{\mu\nu} = \frac{1}{2}(\partial_\sigma\partial_\nu h_\mu^\sigma + \partial_\sigma\partial_\mu h_\nu^\sigma - \partial_\mu\partial_\nu h - \nabla^2 h_{\mu\nu}), \quad (2.33)$$

which for the 00-component becomes

$$R_{00} = \frac{1}{2}(-\nabla^2 h_{00}). \qquad (2.34)$$

Using Eq. (2.34) in (2.32), we find

$$\nabla^2 h_{00} = -\frac{32}{3}\pi G\rho + \frac{1}{3}R. \qquad (2.35)$$

Setting $\rho = M\delta(\vec{r})$ and using (2.30) in (2.35), we obtain the solution for h_{00} as

$$h_{00} = \frac{2GM}{r}\left(1 + \frac{1}{3}e^{-mr}\right), \qquad (2.36)$$

which is identical with the corresponding result (2.17) found using the massive BD formalism. In order to find the

$h_{ij}|_{i=j}$ components, we express R in terms of the linearized metric components as

$$R = -2\nabla^2 h_{ij}|_{i=j} + \nabla^2 h_{00}. \qquad (2.37)$$

Using (2.35) in (2.37), we find

$$\nabla^2 h_{ij}|_{i=j} = -\frac{16}{3}\pi G\rho - \frac{1}{3}R, \qquad (2.38)$$

which for $\rho = M\delta(\vec{r})$ and R from Eq. (2.30) leads to

$$h_{ij} = \frac{2GM}{r}\delta_{ij}\left(1 - \frac{1}{3}e^{-mr}\right). \qquad (2.39)$$

This is identical to the corresponding result (2.18) obtained using the massive BD formalism. The generalized Newtonian potential and the PPN parameter γ are now obtained in exactly the same way as in the massive BD formalism.

For $m^2 < 0$, the solution reduces to the oscillating form

$$h_{00} = \frac{2GM}{r}\left(1 + \frac{1}{3}\cos(|m|r + \theta)\right), \qquad (2.40)$$

$$h_{ij} = \frac{2GM}{r}\delta_{ij}\left(1 - \frac{1}{3}\cos(|m|r + \theta)\right). \qquad (2.41)$$

We thus conclude that the two formalisms are consistent and equivalent, and they predict an oscillating correction to the Newtonian potential in accordance with Eq. (2.26) for $m^2 < 0$.

1. Stability at the nonlinear level

We now discuss the stability of this oscillating weak-field solution in the $f(R)$ formulation in the presence of nonlinear terms. Using the ansatz (2.3) in the trace of the dynamical equations (2.27), we find [33]

$$-\ddot{R} + \nabla^2 R + \frac{1}{6}R^2 - m^2 R = -8\pi GMm^2\delta(\vec{r}). \qquad (2.42)$$

For large but finite m^2, the linear term dominates and this equation reduces to Eq. (2.29) with the solution in Eqs. (2.30) and (2.31).

In order to test the stability of this solution, we perturb it, setting $R = \bar{R} + \delta R$, where δR is a time-dependent perturbation. In view of the fact that the unperturbed solution $\bar{R}$ is large $[O(m^2)]$, we need to take into account the back-reaction from the nonlinear term $\frac{1}{6}R^2$ to find the time evolution of the perturbation δR. This contribution has not been taken into account in previous stability analyses [33]. Thus, taking this term into account and keeping only linear terms in δR, we obtain

$$-\delta\ddot{R} + \nabla^2\delta R - m^2\left(1 - \frac{1}{3m^2}\bar{R}\right)\delta R = 0, \qquad (2.43)$$

where $\bar{R}$ is given by Eq. (2.30).

Assuming $m^2 < 0$ and setting $\delta R = \delta R_0(r)e^{\omega t}$, we obtain a Schrodinger-like equation for the perturbation δR_0 of the form

$$(-\nabla^2 + V(r))\delta R_0 = -\omega^2\delta R_0, \qquad (2.44)$$

where the potential is

$$V(r) \equiv m^2\left[1 - \frac{r_c}{3r}\cos(|m|r + \theta)\right] \qquad (2.45)$$

with $r_c \equiv 2GM$. After a rescaling $|m|r \rightarrow \bar{r}$, we are left with a single dimensionless parameter, $\bar{r}_c \equiv |m|r_c$. The presence of the large nontrivial background solution combined with the presence of the nonlinear term has modified the effective mass by an oscillating r-dependent term which is not smaller than the homogeneous mass term. This term could in principle modify the stability properties of the background oscillating solution $\bar{R}$. Notice, however, that such a term would not change the stability properties of the vacuum ($\bar{R} = 0$). We have shown by numerical solution of Eq. (2.44) that there are unstable mode solutions ($\omega^2 > 0$) for all values of the dimensionless parameter $\bar{r}_c$ which rise exponentially with time for finite $\bar{r}$ and go to 0 at $\bar{r} \rightarrow \infty$.

In order to demonstrate the effects of the nonlinear term on the stability of the perturbations, we have solved Eq. (2.43) with the initial conditions $\delta R(t = 0, r) = e^{-r^2}$, $\dot{\delta R}(t = 0, r) = 0$ for both $m^2 > 0$ (stability) and $m^2 < 0$ (instability). For $m^2 > 0$ and proper rescaling, Eq. (2.43) takes the form

$$-\delta\ddot{R} + \nabla^2\delta R - \left(1 - \frac{\bar{r}_c}{3\bar{r}}e^{-r}\right)\delta R = 0, \qquad (2.46)$$

while for $m^2 < 0$ it can be written as

$$-\delta\ddot{R} + \nabla^2\delta R + \left(1 - \frac{\bar{r}_c}{3\bar{r}}\cos(r)\right)\delta R = 0, \qquad (2.47)$$

where we have set the arbitrary phase θ to 0. In order to demonstrate the effects of the nonlinear term on the evolution of the perturbations, we have considered the cases $\bar{r}_c = 0$ (continuous lines in Fig. 2) and $\bar{r}_c = 10$ (dashed lines in Fig. 2). The evolution of the perturbations is shown in Fig. 2 for $m^2 > 0$ (red lines) and $m^2 < 0$ (blue lines). Clearly, the evolution of the perturbations is significantly affected by the presence of the nonlinear term (dashed lines), but it appears that in this case, this term cannot change the stability properties. In different forms of
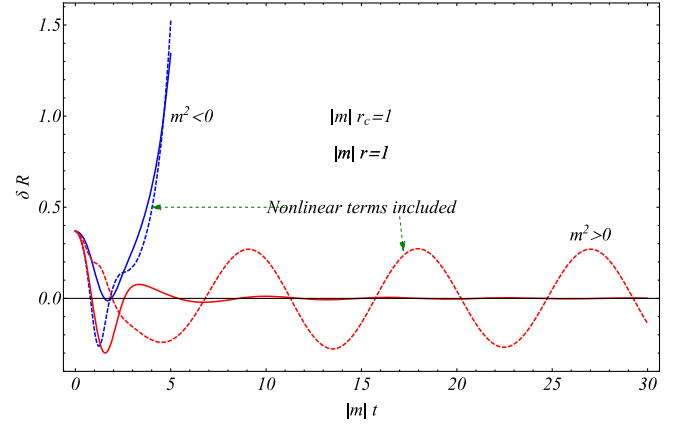

FIG. 2. The evolution of the Ricci scalar perturbations $\delta R(t, |m|r = 1)$ is shown in for $m^2 > 0$ (red lines: stability) and $m^2 < 0$ (blue lines: instability). The dashed lines correspond to the presence of the nonlinear term with $\bar{r}_c = 10$, while for the continuous lines, the nonlinear term is absent ($\bar{r}_c = 0$).

$f(R)$, the effects of such nonlinear terms may become important enough to stabilize such oscillating solutions or destabilize solutions that are stable at the linear level. Notice, for example, that one effect of the nonlinear term is the increase of the amplitude of the oscillations in the stable solution ($m^2 > 0$), thus leading to time-dependent oscillating terms which do not decay even though $m^2 > 0$. This is an interesting new effect with possible cosmological implications [86,87] and deserves further investigation.

C. Nonlocal gravity theories

An important problem of GR is its behavior at small scales, where it predicts the existence of singularities. In addition, at the quantum level, the theory is plagued with unrenormalizable UV divergences (it is not UV-finite) [88]. A possible cure of these divergences is the introduction of higher-derivative terms in the Einstein-Hilbert action, which can make the theory UV-finite [89]. However, such terms introduce instabilities at the quantum level (a spin-2 component of the graviton propagator), which can also destabilize the classical vacuum of the theory. These instabilities can be cured by making the theory nonlocal through the introduction of infinite derivatives in the action leading to modification of the graviton propagator [90]. In order to avoid the introduction of new poles, such infinite derivatives may be introduced in the form of an exponential of an entire function [44,45,91,92].

This class of nonlocal gravity theories generically softens UV divergences at the quantum level while removing the big bang and black hole singularities [90,93]. It also leads to a modification of the Newtonian potential around and below the scale of nonlocality m [41–43,48,94]. This modification includes a removal of the divergence of the potential at $r = 0$ (the potential goes to a constant at $r = 0$) and the possibility of the introduction of decaying spatial

oscillations on scales close to the scale of nonlocality. In particular, the predicted form of the modified Newtonian potential in these theories is of the form [41]

$$V_{\rm eff}(r) = -\frac{GM}{r} f(r, m), \tag{2.48}$$

where

$$f(r, m) = \frac{1}{\pi} \int_{-\infty}^{+\infty} dk \, \frac{\sin(kr) e^{-\tau(k,m)}}{k}. \tag{2.49}$$

A typical form for τ is

$$\tau = \frac{k^{2n}}{m^{2n}}. \tag{2.50}$$

For $n = 1$, it may be shown that $f(r) = Erf(m\frac{r}{2})$, which is linear $\sim r$ for $r < m^{-1}$ and goes to a constant for $r \gg m^{-1}$. The form of $f(r)$ for $n = 1$ and $n = 20$ is shown in Fig. 3 ($\bar{r} \equiv mr$). For $n > 10$, the form of $f(r)$ is practically unchanged. For large n, $f(r)$ is very well fit by the function

$$f(r) = \alpha_1 \bar{r} \quad 0 < \bar{r} < 1, \tag{2.51}$$

$$f(r) = 1 + \alpha_2 \frac{\cos(\bar{r} + \theta)}{\bar{r}} 1 < \bar{r}, \tag{2.52}$$

where $\alpha_1 = 0.544$, $\alpha_2 = 0.572$, and $\theta = 0.885\pi$. Notice the decaying oscillations that develop for $r \gtrsim m^{-1}$ which constitute a signature for this class of models. This class of models are particularly interesting not only for their UV finiteness, but also because they are free from singularities while having a well-defined Newtonian limit in the case $n = 1$. It is therefore important to search for this type
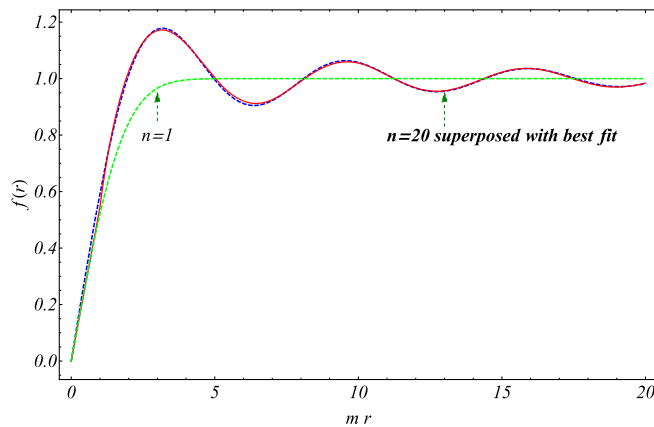

FIG. 3. The form of $f(r)$ for $n = 1$ (dashed green line) and for $n = 20$ superposed with the fit of (2.51) and (2.52). For large n, there are decaying spatial oscillations for $\bar{r} \equiv mr \gtrsim 1$ which are very well fit by (2.51) and (2.52). The linear behavior close to the origin dissolves the divergence of the Newtonian potential.

of spatially oscillating signature in torsion balance experiment data. This type of test is implemented in the next section.

III. OSCILLATING CORRECTIONS ON NEWTON'S CONSTANT: CONSISTENCY WITH MACROSCOPIC OBSERVATIONS AND TORSION BALANCE EXPERIMENTS

A. Observational viability of spatial oscillations of Newton's constant

The generalized Newtonian force forms predicted in the weak-field limit of the theoretical models discussed in the previous section may be obtained easily by differentiation of the corresponding effective gravitational potentials. For the nonlocal large-n effective potential (2.48) fit by Eqs. (2.51) and (2.52), we obtain for $r > m^{-1}$

$$\vec{F}_1 = -\hat{r} \frac{GM}{r^2} \left(1 + \frac{2\alpha_2 \cos(mr + \theta)}{mr} + \alpha_2 \sin(mr + \theta) \right), \tag{3.1}$$

while for the oscillating effective potential (2.26) obtained for $f(R)$ theories, we have

$$\vec{F}_2 = -\hat{r} \frac{GM}{r^2} \left(1 + \frac{\cos(mr + \theta)}{3} + \frac{mr}{3} \sin(mr + \theta) \right). \tag{3.2}$$

The radial weak-field geodesic equation for a bound system in such a force field, after proper rescaling, is of the form

$$\ddot{r} = \frac{1}{r^3} - \frac{1}{r^2} \left(1 + \frac{1}{3} \cos(mr + \theta) + \frac{1}{3} mr \sin(mr + \theta) \right). \tag{3.3}$$

This equation may be obtained using the effective potential

$$V(r) = \frac{1}{2r^2} - \frac{1}{r} \left(1 + \frac{1}{3} \cos(mr + \theta) \right), \tag{3.4}$$

which is shown in Fig. 4 along with the corresponding Newtonian effective potential of a bound system.

Both types of forces, (3.1) and (3.2), clearly do not have a Newtonian limit, since as $m \to \infty$, there is no well-defined limit for the corresponding deviations. However, the existence of a Newtonian limit is not the relevant question for the viability of these predictions. The relevant question is the following: What are the experimental and observational consequences of the above forms of gravitational forces for

$$m > 10 \text{ mm}^{-1}, \tag{3.5}$$
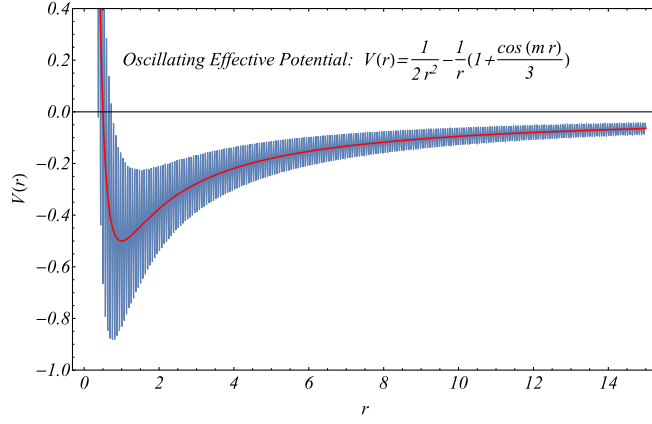
FIG. 4. The oscillating effective potential for a bound system of Eq. (3.4) with $m = 100$, superposed with the corresponding Newtonian potential (red line).

and are these consistent with current experiments and observations?

The fact that the extra spatially oscillating force component averages out to 0 over scales larger than 1 mm makes the answer to this question a nontrivial issue. Immediately ruling out these oscillating gravitational force forms just because they do not have a Newtonian limit would be like ruling out quantum theory because it predicts that macroscopic objects have a wave nature before checking if their de Broglie wavelength is consistent with experiments.

As a simple useful toy model system where the detectability of the predicted force oscillations can be tested, consider a point mass at the center of a thick, homogeneous, spherical shell of density ρ_{sh} with inner radius r_1 and outer radius r_2 (Fig. 5). Consider now the magnitude of the force exerted by a small solid angle $\Delta\Omega$ of the shell. Using Eq. (3.2) [where the oscillating terms are more important compared to the corresponding terms in Eq. (3.1)], we can easily find the force magnitude per solid angle exerted by the shell on the particle as
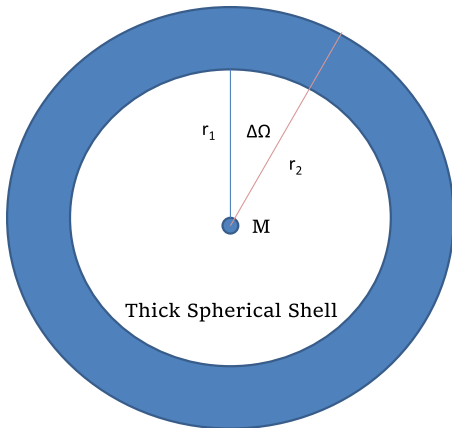

FIG. 5. A point mass interacting gravitationally with a thick massive spherical shell.

$$F_{tot} = F_N + F_a + F_b, \tag{3.6}$$

where F_N is the Newtonian contribution and F_a, F_b are the contributions from the oscillating components which are of the form

$$F_N(r_1, r_2) = GM\rho_{sh}(r_2 - r_1), \tag{3.7}$$

$$F_a(r_1, r_2) = GM\rho_{sh}\frac{2}{m}(\sin(mr_2) - \sin(mr_1)), \tag{3.8}$$

$$F_b(r_1, r_2) = GM\rho_{sh}(r_2\cos(mr_2) - r_1\cos(mr_1)). \tag{3.9}$$

For large r_i and a thin shell, we can have $F_b \gg F_N$, and thus it would appear that the oscillating contribution contradicts all current experiments and observations. However, what is actually measured in any experiment or observation is an *average* gravitational force over a range of distances and object dimensions. This averaging is due to the relative motion of objects during an observation and also due to the inaccurate knowledge of distances and dimensions of gravitating objects, or even due to the quantum uncertainty principle. Thus, the observable gravitational force is

$$\bar{F} = \frac{1}{\delta r^2}\int_{r_1-\delta r/2}^{r_1+\delta r/2}\int_{r_2-\delta r/2}^{r_2+\delta r/2} dr_1' dr_2' F(r_1', r_2'), \tag{3.10}$$

where δr is the uncertainty in r_1, r_2 due to the above mentioned factors. It is straightforward to show that for any finite r_1, r_2, δr and large enough m, the ratios of the oscillating components over the Newtonian component obey

$$\frac{\bar{F}_b}{\bar{F}_N} \lesssim O((m\delta r)^{-1}), \tag{3.11}$$

$$\frac{\bar{F}_a}{\bar{F}_N} \lesssim O((m\delta r)^{-1}), \tag{3.12}$$

and thus can be made arbitrarily small and consistent with macroscopic observations and experiments. A similar conclusion can be obtained for the oscillating components of Eq. (3.1) for the oscillations coming from the nonlocal gravity theory.

In view of the derived consistency of the predicted oscillating gravitational force terms with macroscopic observations, it is clear that oscillating force signatures of these theories can be searched in laboratory experiments testing the validity of the Newtonian potential at submillimeter scales. The most constraining such experiments to date for the particular types of potentials discussed in the present analysis are the torsion balance experiments of the Washington group [9]. The Newtonian residual torque data obtained by the Washington group have been used to

constrain Yukawa and power-law-type corrections to the Newtonian potential of the form

$$V_{\text{eff}} = -\frac{GM}{r}(1 + \alpha e^{-mr}) \qquad (3.13)$$

and have ruled out values of $m \lesssim 18$ mm^{-1} for $\alpha = 1$ at the 2σ level. The corresponding gravitational force oscillating parametrization is of the form

$$F_{\text{eff}} = -\hat{r}\frac{GM}{r^2}(1 + \alpha e^{-mr} + \alpha mr e^{-mr}). \qquad (3.14)$$

In the next section, we extend the analysis of the Washington group [9], using a oscillating parametrization in addition to the Yukawa one in an attempt to search for oscillating signatures or constraints in the data. We test the validity of our analysis by verifying that we obtain the same bound on m as that of Ref. [9] for the Yukawa parametrization.

B. Fitting spatial oscillations of Newton's constant to the Washington experiment data

1. Maximum likelihood analysis

The Washington experiment used a missing-mass torsion balance instrument, measuring gravitational interaction torques with extreme accuracy. The torques developed between missing masses (holes) present in a torsion pendulum detector and similar holes present in an attractor ring rotating with constant angular velocity.

The differences (residuals) between the measured torques and their expected Newtonian values were recorded in three experiments (I, II, and III) using the same detector but different thicknesses of attractor disks. The attractor thickness in each experiment was chosen in such a way as to reduce systematic errors by comparing the residuals among the three experiments. The residual torques for each experiment as a function of detector-attractor separation were published in three figures (one for each experiment). Experiment I suffered a minor systematic effect (the detector ring was found to be slightly bowed), which was accounted for by modeling the heights of the outer sets of holes to different heights. No such systematic effect was present in experiments II and III.

A total of 87 residual points were shown along with three predicted residual curves [9,11,12,95] that would arise in the context of Yukawa-type deviations [Eq. (3.13)] from the Newtonian potential for three pairs of $(\alpha, \lambda \equiv 1/m)$. Each point referred to the value of the residual torque (measured value minus Newtonian prediction), the attractor-detector distance in mm, and the 1σ error of the residual torque (see Table II in the Appendix).

We have fit the residual torques $\delta\tau \equiv \tau - \tau_N$ measured in each experiment for several attractor-detector separations, using three parametrizations:

$$\delta\tau_1(\alpha', m', r) = \alpha', \qquad (3.15)$$

$$\delta\tau_2(\alpha', m', r) = \alpha' e^{-m'r}, \qquad (3.16)$$

$$\delta\tau_3(\alpha', m', r) = \alpha' \cos\left(m'r + \frac{3\pi}{4}\right), \qquad (3.17)$$

where α', m' are parameters to be fit. We have fixed $\theta' = \frac{3\pi}{4}$, as it provides better fits than other phase choices. The primes are used to avoid confusion with the corresponding unprimed parameters of the deviations from the Newtonian potential [e.g. Eq. (3.13)].

We have used these parametrizations to minimize $\chi^2(\alpha', m')$, defined as

$$\chi^2(\alpha', m') = \sum_{j=1}^{N} \frac{(\delta\tau(j) - \delta\tau_i(\alpha', m', r_j))^2}{\sigma_j^2}, \qquad (3.18)$$

where i refers to the type of parametrization [Eqs. (3.15)–(3.17)], j refers to the jth data point as shown in Table II, and N is the number of data points in each experiment. The 1σ and 2σ contours for two parameters correspond to the curves satisfying $\chi^2(\alpha', m') = \chi^2_{\text{min}} + 2.3$ and $\chi^2(\alpha', m') = \chi^2_{\text{min}} + 6.17$.

The detailed connection between the parametrization parameters $\alpha', m',$ and θ' and the corresponding parameters $\alpha, m,$ and θ of the gravitational potential requires detailed knowledge of parameters of the experimental apparatus which are not available to us. These parameters could be used to obtain a quantitative estimate of the source integral and thus of the gravitational signal. An approximate estimate of this signal for the case of macroscopic interacting disks will be obtained in what follows.

In an effort to bypass the calculation of the source integral in the case of the Yukawa parametrization, we have attempted to make an empirical connection between the parametrization parameters and the gravitational signal parameters using the published residual torque curves [with well-defined best-fit parameters (α', m')] that correspond to three pairs of Yukawa potential parameters (α, m). This empirical relation connects (α', m') with the (α, m) of a Yukawa deviation in the potential and is discussed in detail in the Appendix. It indicates that

$$m' = m, \qquad (3.19)$$

$$\ln\left(\frac{\alpha'}{\alpha}\right) = 5.65 - 3.15\ln(m), \qquad (3.20)$$

where m is in mm^{-1} and α' is in fN · m. We stress that these relations are approximately applicable in the case of the Yukawa parametrization and are not necessarily accurate for the derivation of the gravitational signal in the case of the oscillating parametrization. In what follows, however,

TABLE I. The best-fit value of χ^2 for each parametrization, using the total of 87 data points in the three experiments.

Parametrization	χ^2
$\delta\tau = \alpha'$	85.5
$\delta\tau = \alpha' e^{-m'r}$	85.4
$\delta\tau = \alpha' \cos(m'r + \frac{3\pi}{4})$	70.7

we assume that Eq. (3.19) is applicable also for the oscillating parametrization, which is justified by the approximate estimate of the source integral discussed below.

In Table I we show the best-fit χ^2 values for each parametrization for the combined data set from all three experiments. Notice the significant improvement in the quality of fit by $\Delta\chi^2 \simeq -15$ of the oscillating parametrization obtained with $m \simeq 65$ mm^{-1}, which corresponds to a wavelength $\lambda = \frac{2\pi}{m} \simeq 0.1$ mm (see Fig. 7). This scale is surprisingly close to the dark energy scale $\lambda_{de} \equiv \sqrt{4}\frac{hc}{\rho_{de}} = 0.085$ mm, as discussed in the Introduction.

The 1σ and 2σ contours in the parameter space (α', m') are shown in Fig. 6 (Yukawa parametrization) and in Fig. 7

(oscillating parametrization assuming fixed $\theta' = 3\frac{\pi}{4}$) for each one of the three experiments and for the combined data set of 87 data points.

Lines of constant α obtained using Eq. (3.20) are shown in Fig. 6. For $\alpha = 1$, the line intersects the 2σ contours at $m = m' \simeq 20$ mm^{-1} (for the "all data" plot), thus leading to a 2σ constraint $m \gtrsim 20$ mm^{-1} which is almost identical with the constraint of Ref. [9]. This is a good test for the validity of our analysis and of the empirical calibration relations (3.20) and (3.19).

The value of χ^2 as a function of m for the oscillating parametrization (continuous blue line) and for the Newtonian parametrization (straight red line) is shown in Fig. 8 (left panel). For each value of the spatial frequency m, we have minimized with respect to the amplitude and the phase of the parametrization. Even though the most prominent χ^2 minimum is the one at $m \simeq 65$ mm^{-1}, there are some other notable minima. Two of them have a comparable depth with the fundamental deepest minimum at $m = 65$ mm^{-1}. The spatial frequencies are close to the third harmonic of the fundamental frequency ($m \simeq 195$ mm^{-1} and $m \simeq 202$ mm^{-1}). Even though these two minima would appear to be independent, their corresponding
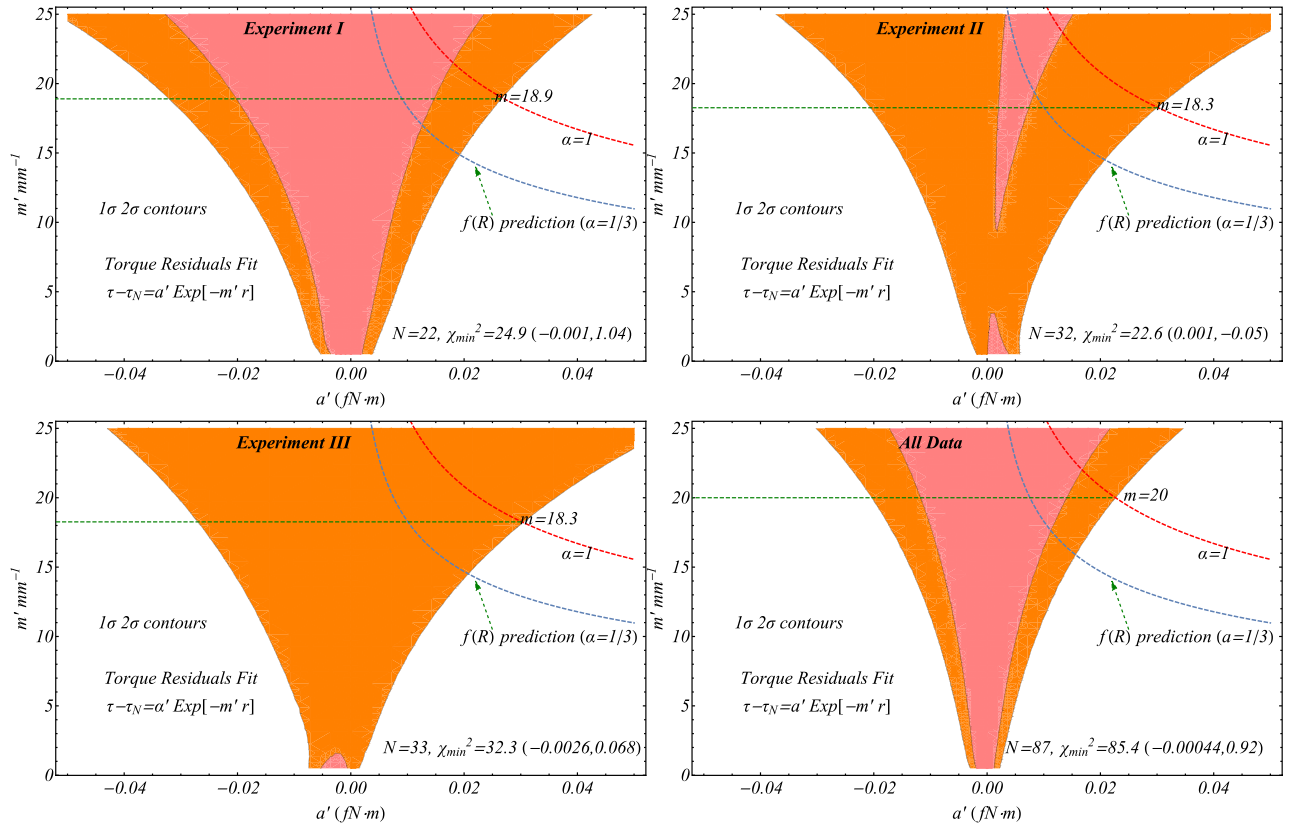

FIG. 6. The 1σ and 2σ contours in the parameter space (α', m') for the Yukawa parametrization. The blue dashed line is the line $\alpha = \frac{1}{3}$ projected onto the parameter space (α', m') in accordance with the empirical relations (3.19) and (3.20). The red line corresponds to $\alpha = 1$ obtained from (3.19) and (3.20) and intersects the 2σ contour at $m \simeq 20$ mm^{-1}, leading to a 2σ constraint $m > 20$ mm^{-1}, in good agreement with the published 2σ constraint on m by the Washington group [9]. This agreement is a good test for the validity of our analysis.
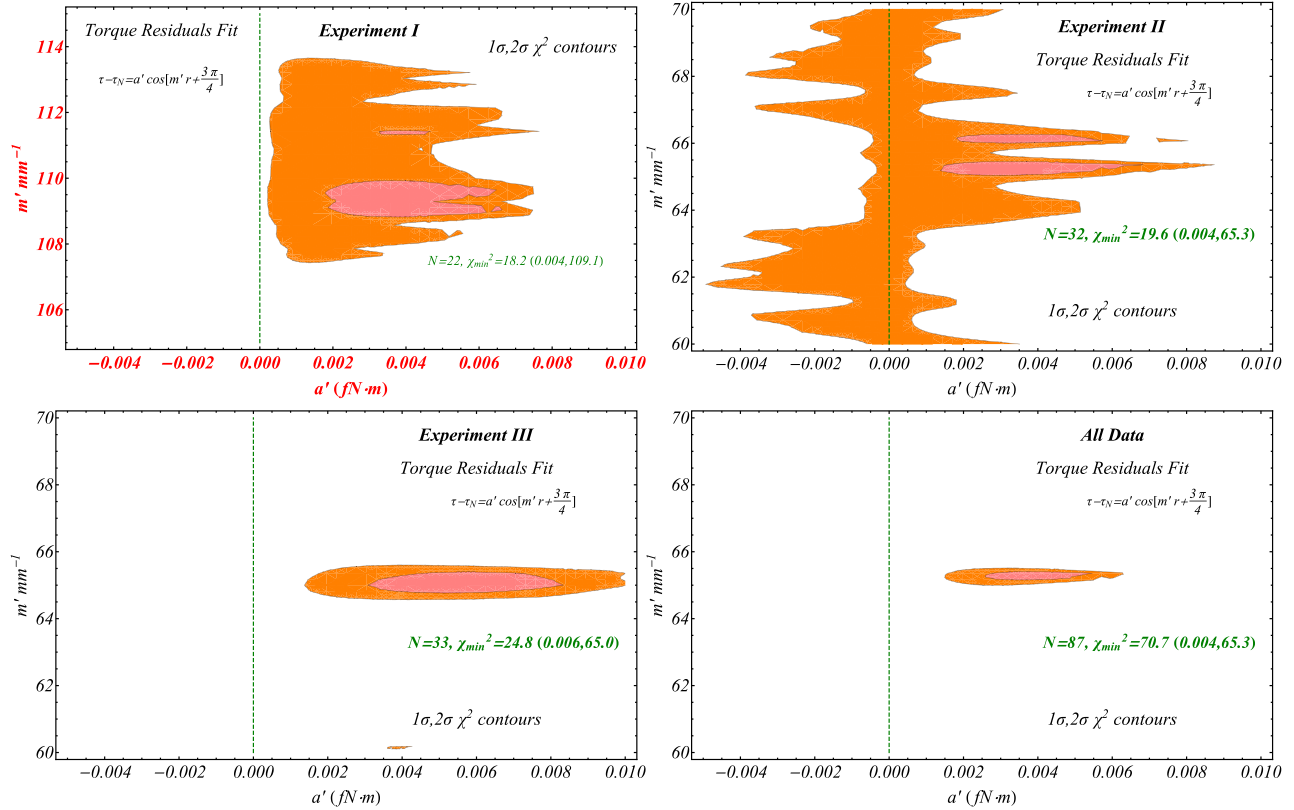
FIG. 7.   The 1σ and 2σ contours in the parameter space (α', m') for the oscillating parametrization with $\theta' = \frac{3\pi}{4}$. Notice that experiment III appears to have the highest constraining power with respect to the oscillating parametrization, while in experiment I the spatial oscillations are best fit by a higher spatial frequency (we used red for the frame label of experiment I to show this distinct behavior). However, even the data of experiment I are well fit by the same spatial frequency as the other two experiments (local minimum of χ^2, as shown in Fig. 8). For the combined data set, there is a well-defined high-quality fit at $(\alpha', m') = (0.004, 65.3)$ corresponding to a wavelength $\lambda = \frac{2\pi}{m} = 0.096$ mm. This best fit is about 3σ away from the null Newtonian value $\alpha' = 0$.

best-fit parametrizations behave as higher harmonics of the fundamental minimum. This is demonstrated in Fig. 9, where it can be seen that the first few roots of the best-fit form of $m \simeq 202$ mm^{-1} coincide with the corresponding roots of the fundamental best fit at $m = 65$ mm^{-1}.

The effects of horizontal uncertainties on the location and depth of the minima, assuming a fixed horizontal error for each data point of $\sigma_r = 0.002$ mm, are shown in Fig. 8 (right panel). In this case, χ^2 is evaluated by adding the term $\left(\frac{\partial \delta\tau}{\partial r}\sigma_r\right)^2$ in the denominator of the expression
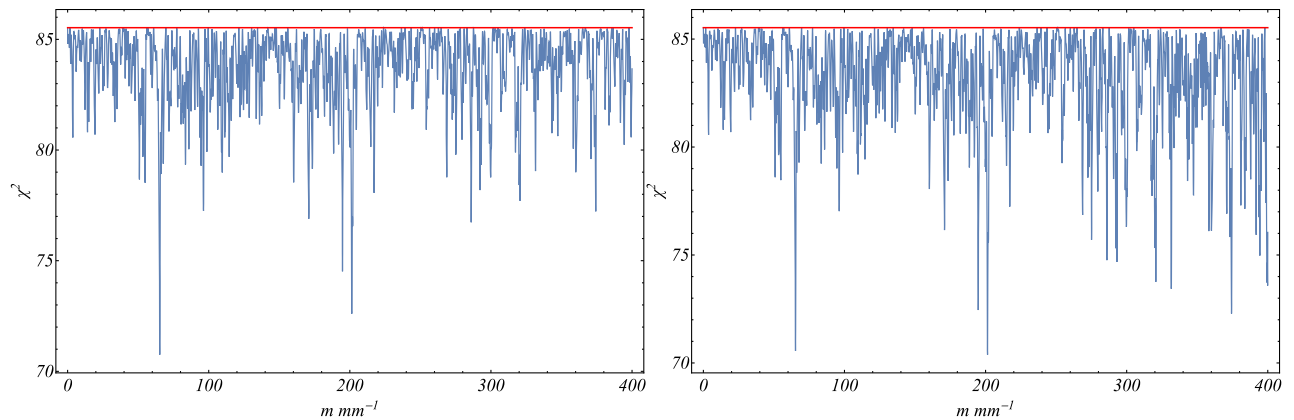

FIG. 8.   The value of the minimized χ^2 as a function of the spatial frequency m without including horizontal uncertainties (left panel) and including horizontal uncertainties $\sigma_r = 0.002$ mm at each data point (right panel). The locations of the minima are not affected, while their depths increase at higher spatial frequencies. The red straight line corresponds to the Newtonian residual $\delta\tau = 0$.
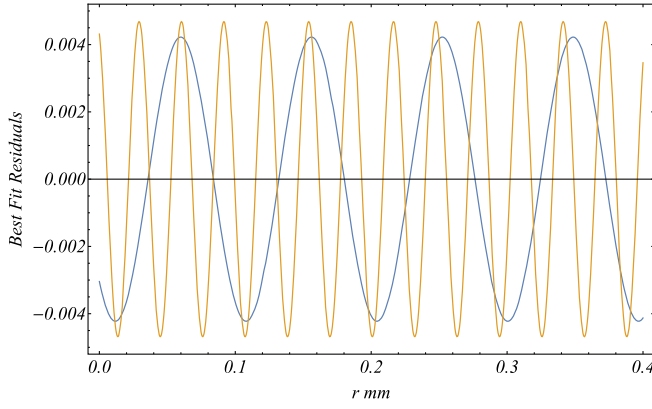
FIG. 9. The best-fit oscillating forms corresponding to the two deepest χ^2 minima ($m \simeq 65$ mm^{-1} and $m \simeq 202$ mm^{-1}). The blue curve, with the larger wavelength, corresponds to a spatial frequency $m = 65$ mm^{-1} with wavelength $\lambda = 2\pi/m \simeq$ 0.097 mm = 97 μm. The (approximate) higher harmonic (brown curve) corresponds to a spatial frequency $m = 202$ mm^{-1} with wavelength $\lambda = 2\pi/m \simeq 0.031$ mm. The roots and maxima of the two curves are correlated, and the second curve (brown) appears as a higher harmonic of the first (blue).

defining χ^2 [Eq. (3.18)]. Thus, the definition of χ^2 becomes

$$\chi^2(\alpha', m') = \sum_{j=1}^{N} \frac{(\delta\tau(j) - \delta\tau(\alpha', m', \theta', r_j))^2}{\sigma_j^2 + (\frac{\partial \delta\tau}{\partial r}\sigma_r)^2}. \quad (3.21)$$

As shown in Fig. 8 (right panel), the locations of the minima are not affected by this introduction of horizontal errors, even though the depths of the higher-frequency minima appear to increase. The depth and location of the fundamental minimum at $m = 65$ mm^{-1} are practically unaffected by taking into account such horizontal errors, since the relevant scale of these errors is much smaller.

The residual torque data along with the best-fit Yukawa and oscillating parametrizations are shown in Fig. 10 for each experiment separately, as well as for the combined data set. The values of χ^2 for the best fit and for the corresponding constant fit (Newtonian plus constant offset) are also shown in each plot.

In view of the presence of the additional minima of χ^2 shown in Fig. 8, it becomes clear that the 3σ level of significance of the $m = 65$ mm^{-1} minimum that emerges from the contour plot of Fig. 7 is an overestimate. In order to obtain a better estimate of the level of significance of this minimum, we have constructed 100 Monte Carlo realizations of the Washington data assuming an underlying Newtonian model. We used the same error bars and r coordinates of the original data and assumed a Gaussian distribution for each data point around a zero mean with standard deviation equal to the data error bars. We then fit these data sets with oscillating parametrizations in the range 0–100 mm^{-1}, which includes the identified

fundamental frequency 65 mm^{-1}, by varying both the amplitude and the phase of the parametrization for each value of the spatial frequency m. We found that about 10% of the deepest minima of the Monte Carlo data sets are deeper than the observed fundamental minimum at $m = 65$ mm^{-1} (see Fig. 11). Thus, even though the oscillating parametrization considered is a viable fit to the data, the level of significance of the corresponding χ^2 minimum is not more than 2σ.

2. Source integral: An estimate of the expected gravitational signal

Our assumption of a harmonic parametrization for the fit of the torque residual data is a simplified approximation based on the theoretically predicted oscillating force forms of Eqs. (3.1) and (3.2) between point particles. In the case of realistic forces between macroscopic bodies, the predicted interaction force is expected to be modified. In the case of the Washington experiments, the relevant macroscopic bodies are disks of approximate radius 2.5 mm and thickness 1 mm corresponding to the missing mass holes of the apparatus.

We have obtained an independent numerical approximate estimate of the residual force that would be present between two disks in the presence of harmonic spatial oscillations of the Newtonian potential. In this calculation we have assumed a modified Newtonian force field motivated by nonlocal gravity [e.g. (3.1)] and discretized each disk to a grid with a large number of segments of scale Δx. Assuming two disks of the same radius R with symmetry axes parallel to the z-axis and centers at the origin and at (x_0, y_0, z_0), respectively, we discretize the radius as $R = \bar{R}\Delta x$ and the height as $2h = 2\bar{h}\Delta x$, where $\bar{R}$ and $\bar{h}$ are integers denoting the dimensions of the disks in units of Δx. The Newtonian force between two cubic segments with central coordinates (x_i, y_i, z_i) [included in the disk centered at the origin] and (x_j, y_j, z_j) [included in the disk centered at (x_0, y_0, z_0)] is of the form

$$
\begin{aligned}
\vec{F}_{ij}^N &= -G\rho_1\rho_2(\Delta x)^6 \frac{\vec{r}_j - \vec{r}_i}{((x_j - x_i)^2 + (y_j - y_i)^2 + (z_j - z_i)^2)^{3/2}} \\
&= -G\rho_1\rho_2(\Delta x)^4 \frac{\vec{r}_j - \vec{r}_i}{((\bar{x}_j - \bar{x}_i)^2 + (\bar{y}_j - \bar{y}_i)^2 + (\bar{z}_j - \bar{z}_i)^2)^{3/2}} \\
&\equiv -G\rho_1\rho_2(\Delta x)^4 \frac{\vec{\bar{r}}_{ij}}{\bar{r}_{ij}^3}, \quad (3.22)
\end{aligned}
$$

where ρ_1, ρ_2 are the disk densities, and the "barred" quantities are integers such that, e.g., $x_i = \bar{x}_i\Delta x_i$. The total force between the disks is simply approximated as

$$\vec{F}_{\text{tot}}^N = \sum_{z_i\min}^{z_i\max} \sum_{z_j\min}^{z_j\max} \sum_{x_i\min}^{x_i\max} \sum_{y_i\min}^{y_i\max} \sum_{x_j\min}^{x_j\max} \sum_{y_j\min}^{y_j\max} \vec{F}_{ij}^N, \quad (3.23)$$
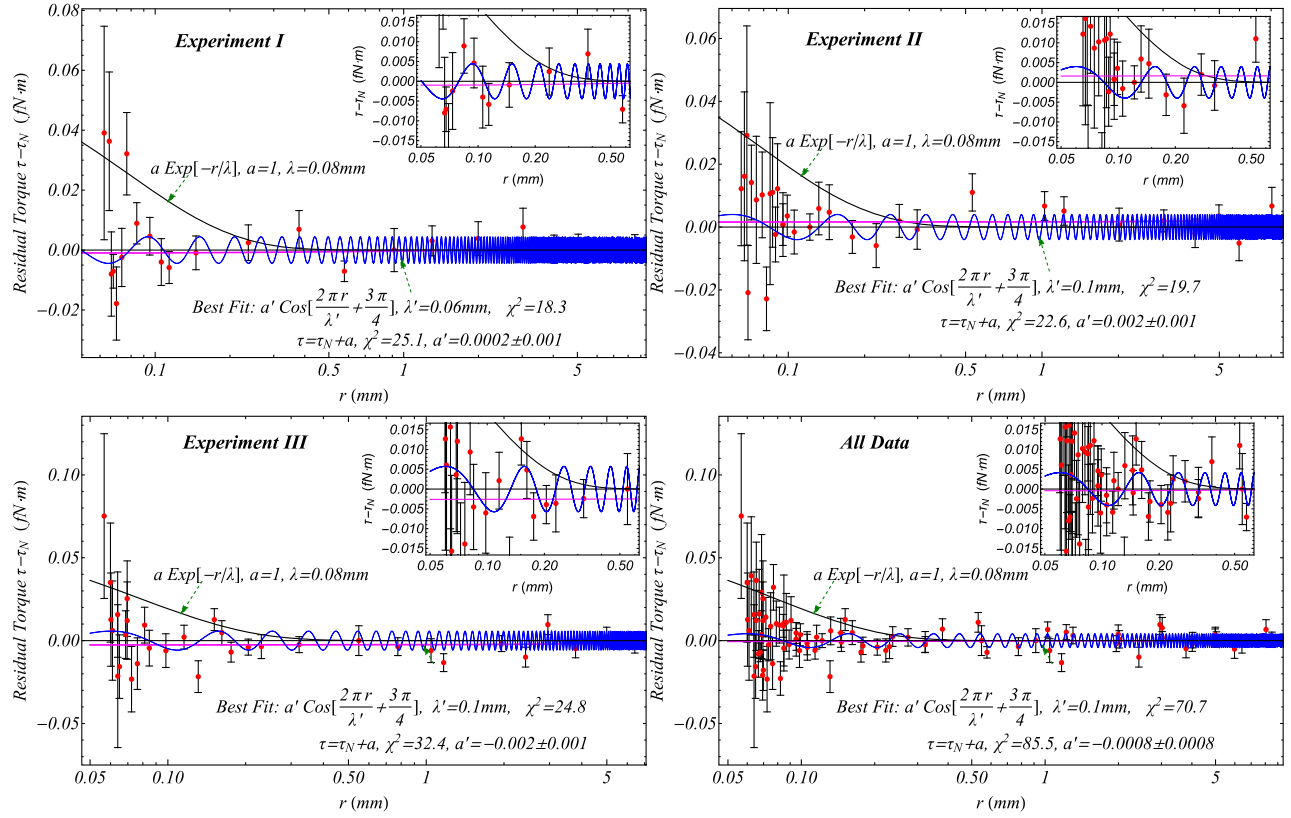
FIG. 10. The residual torque data along with the best-fit Yukawa (thick pink line) and oscillating parametrizations (thin blue line). The Newtonian (with offset) best-fit value and corresponding χ^2 for each best-fit parametrization are also shown.

where the summation limits corresponding to the pair of disks described above are obtained as (in what follows, we omit the "bars")

$$z_{i\,\min} = -h, \tag{3.24}$$
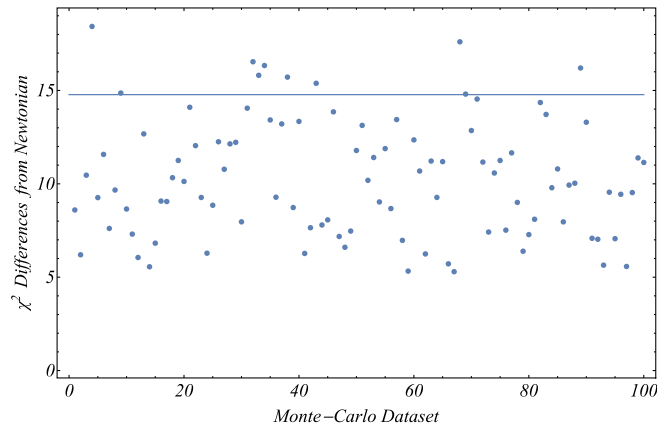
$$z_{i\,\max} = h, \tag{3.25}$$

FIG. 11. The χ^2 differences between the deepest χ^2 in the range $m \in [0, 100]$ and the corresponding Newtonian value of χ^2 in 100 Monte Carlo data sets created under the assumption of zero residuals (Newtonian model).

$$x_{i\,\min} = -R, \tag{3.26}$$

$$x_{i\,\max} = R, \tag{3.27}$$

$$y_{i\,\min} = -\sqrt{R^2 - x_i^2}, \tag{3.28}$$

$$y_{i\,\max} = \sqrt{R^2 + x_i^2}, \tag{3.29}$$

$$z_{j\,\min} = z_0 - h, \tag{3.30}$$

$$z_{j\,\max} = z_0 + h, \tag{3.31}$$

$$x_{j\,\min} = x_0 - R, \tag{3.32}$$

$$x_{j\,\max} = x_0 + R, \tag{3.33}$$

$$y_{j\,\min} = \left(y_0 - \sqrt{R^2 - (x_0 - x_i)^2}\right), \tag{3.34}$$

$$y_{j\,\max} = \left(y_0 + \sqrt{R^2 + (x_0 - x_i)^2}\right). \tag{3.35}$$

The generalized gravitational force predicted by nonlocal gravity theories is nonzero only for $mr > 1$, and it is of the form

$$\vec{F}^O = -\hat{r}\frac{Gm_im_j}{r^2}\left(1 + \frac{2\alpha_2\cos(mr+\theta)}{mr} + \alpha_2\sin(mr+\theta)\right) \tag{3.36}$$

$$= -G\rho_1\rho_2(\Delta x)^4\frac{\vec{r}_{ij}}{r_{ij}^3}\left(1 + \frac{2\alpha_2\cos(mr_{ij}+\theta)}{mr_{ij}}\right.$$

$$\left. + \alpha_2\sin(mr_{ij}+\theta)\right), \tag{3.37}$$

where $m = \frac{2\pi}{\lambda}$ is the fundamental scale of the theory, and the theoretically predicted parameter values were evaluated in Sec. II as $\alpha_2 = 0.572$ and $\theta = 0.885\pi$. The predicted residual x-component of the force for this class of models may be obtained in dimensionless form as

$$F_{x\text{Res}} \equiv \frac{F_x^O - F_x^N}{F_x^N}, \tag{3.38}$$

and similarly for the y- and z-components. Using these definitions, we evaluate $F_{x\text{Res}}$ and $F_{z\text{Res}}$ as functions of the center of the second disk coordinates z_0 and x_0 for $y_0 = 0$. We have set $R = 10$, $\lambda = 5$, and $h = 0$. The assumed unit is Δx. For example, for $\lambda = 100\ \mu\text{m}$, we would have $\Delta x = 20\ \mu\text{m}$ and $R = 200\ \mu\text{m}$.

For disks with a radius of $R = 2$ mm and thickness $2h = 1$ mm, we would have to set up a grid with $R = 100$ and $h = 25$ for the same value of Δx which is needed for proper probing of the oscillations (at least 5 grid points per spatial oscillation wavelength). This calculation would take 5000^2 times longer to run than the calculation for the parameters used above, which makes such a choice impractical. The above implemented choice of dimensions, however, also provides fairly useful insight about the predicted signal.

The choice of disk parameters used corresponds to the division of each disk into a grid with more than 300 segments while thickness is ignored. The assumed spatial wavelength of the oscillating potential is half the radius of the disk. These assumptions allow this simple code to give results in a relatively short time for a wide range of relative positions between the disks. These results are shown in Figs. 12 and 13. In Fig. 12, we show a density plot of the predicted residual force x- and z-components, while in Fig. 13, we show the same components when the second disk is placed along particular spatial directions parallel to the axes of the disks (z-direction). Despite the qualitative nature of this approach, it leads to four interesting conclusions:

(1) The predicted signal for the force between macroscopic bodies remains oscillatory, but for distances comparable to the disk dimensions, it is not a harmonic function with constant amplitude.

(2) The amplitude of the oscillating force on scales smaller than the macroscopic bodies is suppressed compared to the amplitude of the fundamental potential oscillations.

(3) The spatial frequency of the macroscopic force is about the same as the frequency of the fundamental oscillations.

(4) The magnitude of the residual of the oscillating force defined in Eq. (3.38) tends to increase slowly with distance. We have verified that the magnitude of the oscillating force tends to its pointlike value ($a_2 = 0.572$) at large distances between the disks, as expected. As shown in Figs. 12 and 13, the signal also exists off axis even though it is reduced compared to the signal when the symmetry axes of the two disks coincide.
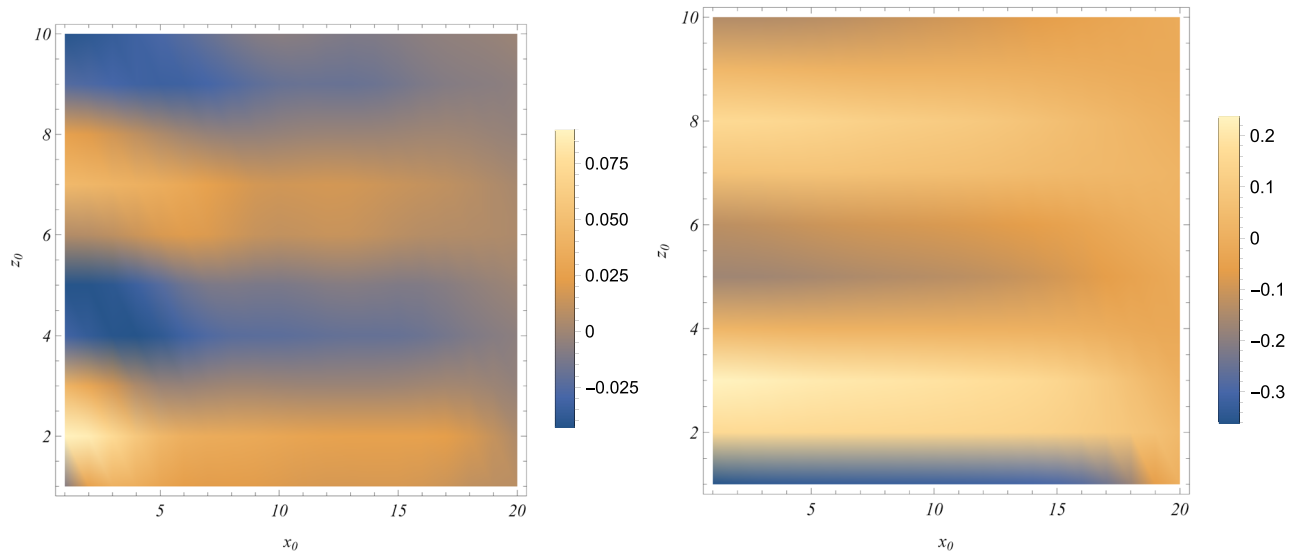

FIG. 12. The residual x (left) and z (right) dimensionless force components for disk radius $R = 10\Delta x$ and oscillation wavelength $\lambda = 5\Delta x$. The axes' units are Δx.
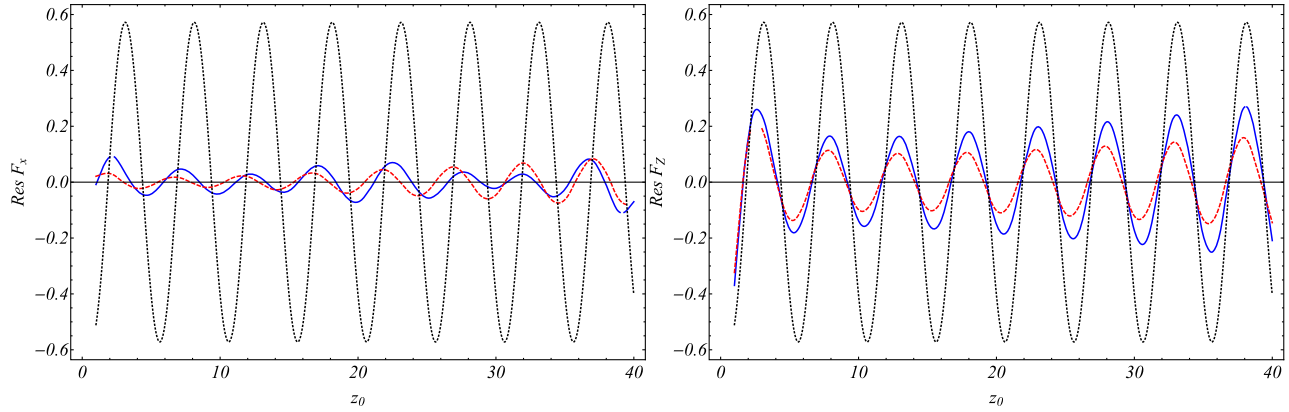
FIG. 13.   The residual x (left) and z (right) dimensionless force components for disk radius $R = 10\Delta x$, $\lambda = 5\Delta x$. The axes' units are Δx. The blue line for the x-component (left panel) corresponds to $x_0 = 1$, while the red line corresponds to $x_0 = 10$. The blue line for the z-component (right panel) corresponds to $x_0 = 0$, while the red line corresponds to $x_0 = 10$. The black line corresponds to the naively expected signal $a\cos(0.5z_0 + \theta)$. (We used $\theta = 3\pi/4$ for the z-component, which seems to fit both the theoretically predicted and the observed signal.) Notice the predicted suppression of the signal at low distances z_0 and its slow increase of the predicted residual with distance. It may be shown that the amplitude grows up to the maximum value of 0.57 as expected, since at large distances the disks behave as pointlike particles.

Based on the above conclusions, an experiment designed to detect spatial oscillations of the gravitational potential should focus on relatively large source-detector distances but vary these distances by small steps comparable to the targeted oscillation wavelength. In this manner the relative residual magnitude of the signal is maximized while the spatial frequency of the signal is properly probed.

IV. CONCLUSIONS-DISCUSSION

We have shown that the presence of submillimeter oscillations of the gravitational potential is a viable possibility at both the theoretical level and the observational/experimental level.

At the theoretical level, we showed that gravitational potential oscillations appear generically in stable extended gravitational theories like nonlocal ghost-free gravity. Even in theories where such oscillations are generic but unstable, we showed that there is potential for stabilization mechanisms induced by nonperturbative effects.

At the macroscopic observational level, we showed that even though these spatial oscillations do not have a strict Newtonian limit, they are consistent with observations and gravitational experiments for small enough values of the wavelength. In fact, we presented evidence that such oscillating parametrizations may provide a better fit to torsion balance data than the Newtonian potential parametrization even though the level of significance of this improvement is not more than 2σ. Our data analysis involved several assumptions and simplifications, especially in the estimate of the source integral. The goal of our data analysis has not been the quantitative estimate of a statistically significant oscillating signature of modified gravity on submilimeter scales. Instead, it has been the

demonstration of the existence of a peculiar oscillating signal in the data which may be statistically significant. This signal could be due to three possible effects:

(1) A statistical fluctuation of the data which is more prominent in experiment III of Ref. [9], as shown in Fig. 7.

(2) A periodic distance-dependent systematic feature in the data. Such an unnoticed class of systematics would not be of wide interest, but it would be notable and useful for the short-distance force measurement community.[2]

(3) An early signal for a short-distance modification of GR. The verification of this possibility would require an extensive, detailed search of short-distance force measurement groups, which will hopefully be motivated by our analysis. Other indications of such oscillating short-distance forces may be seen by eye on the recent data plots (Fig. 3) of Ref. [96].

In view of the possible future verification of the last possibility, the following challenging question needs to be addressed: What is the precise form and amplitude of the theoretically predicted oscillating signal in the context of the Washington experiment? In order to address this question, a calculation of the torque between the pendulum disk and upper attractor for several separations is needed. In the present analysis, we have made some progress for addressing this question at a qualitative level (Sec. III B 2), but the detailed quantitative answer is a challenging issue that remains open and will be addressed in a separate forthcoming analysis. The challenging nature of this question emerges not only because of the small grid spacing required compared to the oscillation wavelength (for which a much larger grid is

---

[2]I thank the referee for pointing this out.

required), but also due to the nonlocal nature of the signal that requires the lower attractor of the Washington experiment to be included in any full calculation.

Our results may have a few interesting implications:

(1) They may be viewed as early evidence for emerging signatures of nonlocal gravity in experimental data. The idea of nonlocal gravity provides one of the very few self-consistent approaches for curing the singularity problems of general relativity while being naturally motivated by the demand of consistency with quantum mechanics. It is remarkable that such a well-motivated extension of general relativity generically predicts the presence of submillimeter spatial oscillations of Newton's constant. The prediction for these oscillations was documented clearly in Ref. [41] and was also seen in Refs. [42,48].

(2) They indicate that oscillating parametrizations for deviations from the Newtonian gravitational potential should be considered along with Yukawa and power-law parametrizations, because they are well motivated theoretically and consistent with macroscopic observations.

(3) They indicate that the stability of $f(R)$ theories that are unstable at the perturbative level could be reexamined by taking into account nontrivial backgrounds and the backreaction from nonlinear terms that act at the nonperturbative level.

Interesting extensions of the present work include the following:

(1) A more detailed analysis of the existence and stability of theoretical models that predict the existence of submillimeter oscillations of the gravitational potential and of Newton's constant. In addition to the models discussed in the present analysis, such models may include the presence of compact timelike extra dimensions [97], brane-world models, etc.

(2) A detailed analysis of the macroscopic effects of submillimeter oscillations of Newton's constant, including possible effects on Solar System scales and/or lunar ranging experiments.

(3) The cosmological effects of such oscillations could also be of significant interest, especially in view of the experimental indications that they may exist with a wavelength close to the dark energy scale. For example, oscillations of Newton's constant in time are generically present in stable scalar-tensor theories and theories with compact extra dimensions and have been shown [86,87] to have interesting cosmological features, including their possible role as dark energy candidates.

(4) The use of alternative parametrizations to fit the torque residual data. It may be possible to find alternative parametrizations that provide better fits, which may provide hints for the construction of new theoretical models. It is also important, however, to identify possible sources of systematics in the data that may induce spurious nonphysical features. For example, the minor systematic effect in experiment I coming from the slightly bowed detector ring could be the origin of the difference of the best-fit spatial wavelength by a factor of 2 found in the data analysis of experiment I.

(5) If the observed signal in the Washington group data is physically interesting, it should leave a signature on other experiments which have the required sensitivity to see the signal (e.g., Refs. [95,96, 98–101]). It is therefore important to extend this analysis to other data sets in an effort to identify similar signatures in other data sets. An investigation along these lines is currently in progress.

In conclusion, we have presented a novel and potentially important result that could motivate further work in the active field of theoretical and experimental searches for the modification of GR.

Numerical Analysis: The Mathematica file that led to the production of the figures may be downloaded from Supplemental Material [102].

APPENDIX: DATA AND ANALYSIS

In this appendix, we describe the derivation of the empirical relations (3.19) and (3.20), and we show the residual torque data used for the fit of the parametrizations considered.
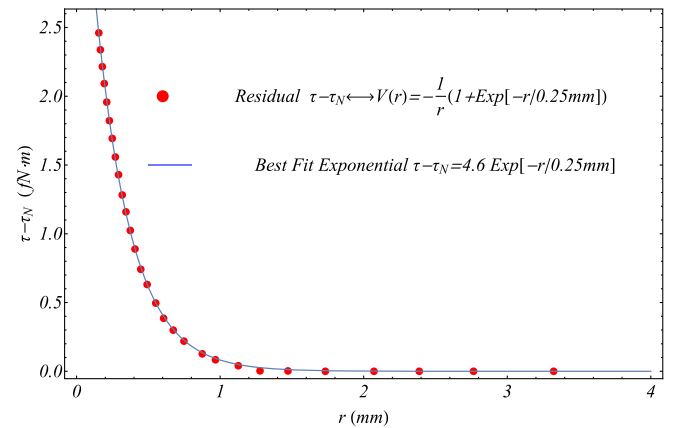

FIG. 14. The curve describing a Yukawa deviation from the Newtonian potential in the torque residuals (thick dots) is fit well as an exponential with the same value of m (continuous line).
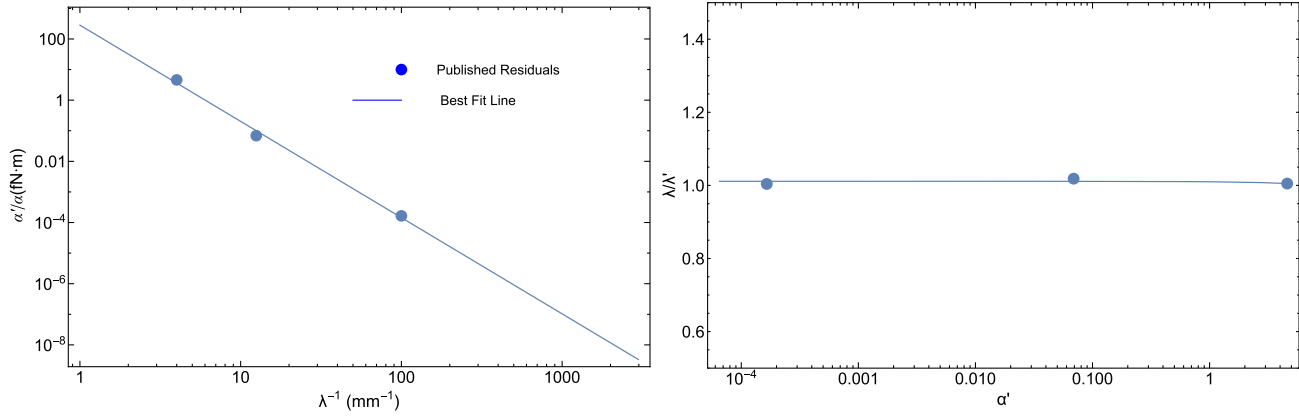
FIG. 15. Using three plots like the one shown in Fig. 14, we may relate the parameters (α, m) of the potential deviations with the corresponding parameters (α', m') in the space of torque residuals fit with the same parametrization. These plots demonstrate the validity of Eqs. (3.19) and (3.20) (continuous lines through points).

In order to calibrate the measured torque residuals and connect them with the parameters of the deviations from the Newtonian potential [α and m of Eq. (3.13)], we use the published residual torque curves that correspond to Yukawa-type Newtonian deviations for specific parameter values. We find that these residual curves are very well fit by exponentials with the same exponents as the exponents of the Yukawa Newtonian potential deviations. This is consistent with Eq. (3.14), which implies that the dominant residual torque for $mr > 1$ is

$$\tau - \tau_N \sim e^{-mr}. \tag{A1}$$

This exponential behavior of the residual torque is verified in Fig. 14, where we show the form published in Ref. [12] of the residual torque (thick dots) corresponding to a Yukawa deviation with $\alpha = 1$ and $\lambda \equiv m^{-1} = 0.25$ mm superposed with the best-fit exponential $\alpha' e^{-r/\lambda'}$. As expected, we find an excellent fit for $\lambda' = \lambda = 0.25$ mm. Also, since $\alpha = 1$ and the best fit is $\alpha' = 4.6$, we have $\frac{\alpha'}{\alpha} = 4.6$.

Using also the other two similar residual torque curves of Ref. [9] for $(\alpha, m^{-1}) = (1, 0.08$ mm$)$ and $(\alpha, m^{-1}) = (10^5, 0.01$ mm$)$, we evaluate the corresponding ratios $\frac{\lambda}{\lambda'}$ and $\frac{\alpha'}{\alpha}$ and thus construct Fig. 15. Using a proper fit to these points, we derive the empirical relations (3.20), (3.19), which relate (α, m) with (α', m').

Finally, in Table II, we show the data points used to find the best fit for the three parametrizations (3.15), (3.16), and (3.17). These data points, obtained from Figs. 3, 4, and 5 of Ref. [9] using plot-digitizer software,[3] are shown in Table II. The uncertainties in the measurement of r in the data of Table II is in the range of 0.002–0.005 mm, which is much smaller than the scale of the oscillation signal. As shown in Fig. 8, the uncertainties of r in this range leave the χ^2 minima in the range around $m \in [0, 100]$ mm^{-1} practically unaffected.

TABLE II. The residual torque 87 data points used for the χ^2 analysis.

$r\,mm$	$\tau - \tau_N$ (fN · m)	$1\sigma(\tau - \tau_N)$	Experiment
0.062	0.039	0.036	I
0.065	0.036	0.023	I
0.067	−0.008	0.014	I
0.068	−0.007	0.006	I
0.07	−0.018	0.012	I
0.073	−0.002	0.01	I
0.077	0.032	0.014	I
0.084	0.009	0.007	I
0.095	0.005	0.006	I
0.106	−0.004	0.008	I
0.114	−0.006	0.005	I
0.146	−0.001	0.006	I
0.237	0.002	0.006	I
0.379	0.007	0.006	I
0.577	−0.007	0.003	I
0.915	0.	0.007	I
1.301	0.003	0.005	I
1.995	0.004	0.006	I
3.021	0.008	0.006	I
4.027	0.	0.005	I
5.04	0.001	0.004	I
8.512	0.001	0.004	I
0.065	0.012	0.018	II
0.067	0.016	0.027	II
0.069	0.029	0.035	II
0.069	−0.021	0.015	II
0.072	0.014	0.012	II
0.075	0.009	0.02	II
0.079	0.01	0.014	II
0.082	−0.023	0.01	II
0.085	0.011	0.029	II
0.087	0.011	0.017	II
0.089	−0.002	0.009	II
0.091	0.012	0.014	II
0.095	0.001	0.01	II

(Table continued)

[3]http://arohatgi.info/WebPlotDigitizer/

TABLE II. *(Continued)*

rmm	$\tau - \tau_N$ (fN · m)	$1\sigma(\tau - \tau_N)$	Experiment
0.095	0.001	0.007	II
0.099	0.004	0.007	II
0.106	−0.002	0.007	II
0.122	0.	0.004	II
0.132	0.006	0.008	II
0.145	0.005	0.009	II
0.179	−0.003	0.005	II
0.222	−0.006	0.007	II
0.274	0.002	0.005	II
0.322	−0.001	0.006	II
0.531	0.011	0.006	II
1.024	0.007	0.005	II
1.221	0.005	0.005	II
2.014	0.001	0.005	II
3.021	0.002	0.003	II
4.014	−0.002	0.005	II
4.983	0.004	0.004	II
5.981	−0.005	0.006	II
8.054	0.007	0.006	II
0.057	0.075	0.05	III
0.06	0.035	0.036	III
0.06	0.013	0.028	III
0.061	0.006	0.03	III
0.064	0.016	0.026	III
0.064	−0.021	0.043	III
0.065	−0.016	0.019	III

TABLE II. *(Continued)*

rmm	$\tau - \tau_N$ (fN · m)	$1\sigma(\tau - \tau_N)$	Experiment
0.069	0.004	0.014	III
0.07	0.012	0.023	III
0.07	0.025	0.023	III
0.072	−0.023	0.02	III
0.076	−0.014	0.016	III
0.081	0.009	0.011	III
0.085	−0.005	0.011	III
0.098	−0.006	0.01	III
0.116	0.002	0.007	III
0.131	−0.022	0.01	III
0.151	0.013	0.007	III
0.162	0.005	0.007	III
0.176	−0.007	0.006	III
0.205	−0.004	0.005	III
0.23	−0.004	0.007	III
0.322	−0.002	0.005	III
0.548	0.	0.009	III
0.777	−0.004	0.005	III
1.044	−0.006	0.007	III
1.168	−0.013	0.005	III
1.958	−0.002	0.005	III
2.423	−0.01	0.006	III
2.957	0.01	0.006	III
3.784	−0.005	0.006	III
4.993	0.002	0.006	III
6.416	−0.002	0.005	III

(Table continued)

[1] A. G. Riess *et al.* (Supernova Search Team Collaboration), Astron. J. **116**, 1009 (1998).

[2] P. J. E. Peebles and B. Ratra, Rev. Mod. Phys. **75**, 559 (2003).

[3] R. R. Caldwell and M. Kamionkowski, Annu. Rev. Nucl. Part. Sci. **59**, 397 (2009).

[4] E. J. Copeland, M. Sami, and S. Tsujikawa, Int. J. Mod. Phys. D **15**, 1753 (2006).

[5] T. Clifton, P. G. Ferreira, A. Padilla, and C. Skordis, Phys. Rep. **513**, 1 (2012).

[6] S. Nojiri and S. D. Odintsov, TSPU Bull. **N8(110)**, 7 (2011).

[7] L. Amendola *et al.*, arXiv:1606.00180.

[8] S. Capozziello and M. De Laurentis, Phys. Rep. **509**, 167 (2011).

[9] D. J. Kapner, T. S. Cook, E. G. Adelberger, J. H. Gundlach, B. R. Heckel, C. D. Hoyle, and H. E. Swanson, Phys. Rev. Lett. **98**, 021101 (2007).

[10] J. Murata and S. Tanaka, Classical Quantum Gravity **32**, 033001 (2015).

[11] C. D. Hoyle, D. J. Kapner, B. R. Heckel, E. G. Adelberger, J. H. Gundlach, U. Schmidt, and H. E. Swanson, Phys. Rev. D **70**, 042004 (2004).

[12] C. D. Hoyle, U. Schmidt, B. R. Heckel, E. G. Adelberger, J. H. Gundlach, D. J. Kapner, and H. E. Swanson, Phys. Rev. Lett. **86**, 1418 (2001).

[13] E. G. Adelberger, B. R. Heckel, S. A. Hoedl, C. D. Hoyle, D. J. Kapner, and A. Upadhye, Phys. Rev. Lett. **98**, 131104 (2007).

[14] A. Donini and S. G. Marimón, Eur. Phys. J. C **76**, 696 (2016).

[15] R. Benichou and J. Estes, Phys. Lett. B **712**, 456 (2012).

[16] K. A. Bronnikov, S. A. Kononogov, and V. N. Melnikov, Gen. Relativ. Gravit. **38**, 1215 (2006).

[17] S. Nojiri and S. D. Odintsov, Phys. Lett. B **548**, 215 (2002).

[18] C. P. L. Berry and J. R. Gair, Phys. Rev. D **83**, 104022 (2011); **85**, 089906(E) (2012).

[19] S. Capozziello, A. Stabile, and A. Troisi, Mod. Phys. Lett. A **24**, 659 (2009).

[20] G. O. Schellstede, Gen. Relativ. Gravit. **48**, 118 (2016).

[21] L. Perivolaropoulos, Phys. Rev. D **81**, 047501 (2010).

[22] M. Hohmann, L. Jarv, P. Kuusk, and E. Randla, Phys. Rev. D **88**, 084054 (2013); **89**, 069901(E) (2014).

[23] L. Järv, P. Kuusk, M. Saal, and O. Vilson, Phys. Rev. D **91**, 024041 (2015).

[24] N. Arkani-Hamed, S. Dimopoulos, and G. R. Dvali, Phys. Lett. B **429**, 263 (1998).

[25] N. Arkani-Hamed, S. Dimopoulos, and G. R. Dvali, Phys. Rev. D **59**, 086004 (1999).

[26] I. Antoniadis, N. Arkani-Hamed, S. Dimopoulos, and G. R. Dvali, Phys. Lett. B **436**, 257 (1998).

[27] L. Perivolaropoulos and C. Sourdis, Phys. Rev. D **66**, 084018 (2002).

[28] E. G. Floratos and G. K. Leontaris, Phys. Lett. B **465**, 95 (1999).

[29] A. Kehagias and K. Sfetsos, Phys. Lett. B **472**, 39 (2000).

[30] S. Capozziello, A. Stabile, and A. Troisi, Phys. Rev. D **76**, 104019 (2007).

[31] G. J. Olmo, Phys. Rev. D **72**, 083505 (2005).

[32] A. D. Dolgov and M. Kawasaki, Phys. Lett. B **573**, 1 (2003).

[33] V. Faraoni, Phys. Rev. D **74**, 104017 (2006).

[34] S. Nojiri and S. D. Odintsov, Phys. Rev. D **68**, 123512 (2003).

[35] S. Capozziello, M. De Laurentis, and V. Faraoni, Open Astron. J. **3**, 49 (2010).

[36] V. Faraoni, Phys. Rev. D **75**, 067302 (2007).

[37] I. Navarro and K. Van Acoleyen, J. Cosmol. Astropart. Phys. 02 (2007) 022.

[38] V. Faraoni and N. Lanahan-Tremblay, Phys. Rev. D **77**, 108501 (2008).

[39] S. Nojiri and S. D. Odintsov, Phys. Lett. B **652**, 343 (2007).

[40] G. Cognola, E. Elizalde, S. Nojiri, S. D. Odintsov, L. Sebastiani, and S. Zerbini, Phys. Rev. D **77**, 046009 (2008).

[41] J. Edholm, A. S. Koshelev, and A. Mazumdar, Phys. Rev. D **94**, 104033 (2016).

[42] A. Kehagias and M. Maggiore, J. High Energy Phys. 08 (2014) 029.

[43] V. P. Frolov and A. Zelnikov, Phys. Rev. D **93**, 064048 (2016).

[44] E. T. Tomboulis, arXiv:hep-th/9702146.

[45] W. Siegel, arXiv:hep-th/0309093.

[46] T. Biswas, A. Conroy, A. S. Koshelev, and A. Mazumdar, Classical Quantum Gravity **31**, 015022 (2014); **31**, 159501(E) (2014).

[47] Y. Dirian, S. Foffa, M. Kunz, M. Maggiore, and V. Pettorino, J. Cosmol. Astropart. Phys. 05 (2016) 068.

[48] M. Maggiore and M. Mancarella, Phys. Rev. D **90**, 023005 (2014).

[49] H. Nersisyan, Y. Akrami, L. Amendola, T. S. Koivisto, J. Rubio, and A. R. Solomon, Phys. Rev. D **95**, 043539 (2017).

[50] S. Talaganis, T. Biswas, and A. Mazumdar, Classical Quantum Gravity **32**, 215017 (2015).

[51] S. Park and S. Dodelson, Phys. Rev. D **87**, 024003 (2013).

[52] G. Calcagni and G. Nardelli, Phys. Rev. D **82**, 123518 (2010).

[53] A. O. Barvinsky, Phys. Lett. B **710**, 12 (2012).

[54] J. Chiaverini, S. J. Smullin, A. A. Geraci, D. M. Weld, and A. Kapitulnik, Phys. Rev. Lett. **90**, 151101 (2003).

[55] S. J. Smullin, A. A. Geraci, J. Chiaverini, D. M. Weld, S. Holmes, and A. Kapitulnik, Phys. Rev. D **72**, 122001 (2005).

[56] A. A. Geraci, S. J. Smullin, D. M. Weld, J. Chiaverini, and A. Kapitulnik, Phys. Rev. D **78**, 022002 (2008).

[57] J. C. Long, H. W. Chan, A. B. Churnside, E. A. Gulbis, M. C. M. Varney, and J. C. Price, Nature (London) **421**, 922 (2003).

[58] V. P. Mitrofanov and O. I. Ponomareva, Sov. Phys. JETP **87**, 1963 (1988).

[59] J. Murata et al., Hyperfine Interact. **225**, 193 (2014).

[60] J. K. Hoskins, R. D. Newman, R. Spero, and J. Schultz, Phys. Rev. D **32**, 3084 (1985).

[61] R. Spero, J. K. Hoskins, R. Newman, J. Pellam, and J. Schultz, Phys. Rev. Lett. **44**, 1645 (1980).

[62] V. I. Panov and V. N. Frontov, Sov. Phys. JETP **50**, 852 (1979).

[63] M. V. Moody and H. J. Paik, Phys. Rev. Lett. **70**, 1195 (1993).

[64] H. Hirakawa, K. Tsubono, and K. Oide, Nature (London) **283**, 184 (1980).

[65] Y. Ogawa, K. Tsubono, and H. Hirakawa, Phys. Rev. D **32**, 342 (1982).

[66] K. Kuroda and H. Hirakawa, Phys. Rev. D **32**, 342 (1985).

[67] N. Mio, K. Tsubono, and H. Hirakawa, Phys. Rev. D **36**, 2321 (1987).

[68] Y. T. Chen, A. H. Cook, and A. J. F. Metherell, Proc. R. Soc. Edinburgh, Sect. A **394**, 47 (1984).

[69] H. A. Chan and M. V. Moody, Phys. Rev. Lett. **49**, 1745 (1982).

[70] S. K. Lamoreaux, Phys. Rev. Lett. **78**, 5 (1997).

[71] A. O. Sushkov, W. J. Kim, D. A. R. Dalvit, and S. K. Lamoreaux, Phys. Rev. Lett. **107**, 171101 (2011).

[72] J. Murata and S. Tanaka, Classical Quantum Gravity **32**, 033001 (2015).

[73] L. C. Tu, S. G. Guan, J. Luo, C. G. Shao, and L. X. Liu, Phys. Rev. Lett. **98**, 201101 (2007).

[74] S. Q. Yang, B. F. Zhan, Q. L. Wang, C. G. Shao, L. C. Tu, W. H. Tan, and J. Luo, Phys. Rev. Lett. **108**, 081101 (2012).

[75] V. K. Milyukov, Sov. Phys. JETP **61**, 187 (1985).

[76] A. De Felice and S. Tsujikawa, Living Rev. Relativ. **13**, 3 (2010).

[77] T. Chiba, T. L. Smith, and A. L. Erickcek, Phys. Rev. D **75**, 124014 (2007).

[78] T. Chiba, Phys. Lett. B **575**, 1 (2003).

[79] S. Capozziello, A. Stabile, and A. Troisi, Phys. Lett. B **686**, 79 (2010).

[80] V. Faraoni, Phys. Rev. D **74**, 023529 (2006).

[81] G. J. Olmo, Phys. Rev. D **75**, 023511 (2007).

[82] A. L. Erickcek, T. L. Smith, and M. Kamionkowski, Phys. Rev. D **74**, 121501 (2006).

[83] O. Bertolami, R. March, and J. Páramos, Phys. Rev. D **88**, 064019 (2013).

[84] S. R. Dolan, Phys. Rev. D **76**, 084001 (2007).

[85] N. Castel-Branco, master's thesis, Lisbon, IST (2014).

[86] P. J. Steinhardt and C. M. Will, Phys. Rev. D **52**, 628 (1995).

[87] L. Perivolaropoulos, Phys. Rev. D **67**, 123516 (2003).

[88] M. H. Goroff and A. Sagnotti, Nucl. Phys. **B266**, 709 (1986).

[89] K. S. Stelle, Gen. Relativ. Gravit. **9**, 353 (1978).

[90] T. Biswas, E. Gerwick, T. Koivisto, and A. Mazumdar, Phys. Rev. Lett. **108**, 031101 (2012).

[91] S. Deser and A. N. Redlich, Phys. Lett. B **176**, 350 (1986); **186**, 461(E) (1987).

[92] L. Modesto, Phys. Rev. D **86**, 044005 (2012).

[93] A. V. Frolov, Phys. Rev. Lett. **101**, 061103 (2008).

[94] M. Hohmann, L. Jarv, P. Kuusk, E. Randla, and O. Vilson, Phys. Rev. D **94**, 124015 (2016).

[95] D. J. Kapner, Ph.D. thesis, Washington University, Seattle (2005).

[96] A. D. Rider, D. C. Moore, C. P. Blakemore, M. Louis, M. Lu, and G. Gratta, Phys. Rev. Lett. **117**, 101101 (2016).

[97] I. Quiros, arXiv:0707.0714.

[98] S.-Q. Yang, B.-F. Zhan, Q.-L. Wang, C.-G. Shao, L.-C. Tu, W.-H. Tan, and J. Luo, Phys. Rev. Lett. **108**, 081101 (2012).

[99] W.-H. Tan, S.-Q. Yang, C.-G. Shao, J. Li, A.-B. Du, B.-F. Zhan, Q.-L. Wang, P.-S. Luo, L.-C. Tu, and J. Luo, Phys. Rev. Lett. **116**, 131101 (2016).

[100] T. Cook, Ph.D. thesis, Washington University, Seattle (2013).

[101] C. A. Hagedorn, Ph.D. thesis, Washington University, Seattle (2015).

[102] See Supplemental Material at http://link.aps.org/supplemental/10.1103/PhysRevD.95.084050 for Mathematica numerical analysis files that were used for the construction of the figures.